Ionic Blockade of the Rat Connexin40 Gap Junction Channel by Large Tetraalkylammonium Ions

Hassan Musa,* Jonathan D. Gough,† Watson J. Lees,† and Richard D. Veenstra*
*Department of Pharmacology, State University of New York, Upstate Medical University, Syracuse, New York 13210 and
†Department of Chemistry, Syracuse University, Syracuse, New York 13244 USA

ABSTRACT The rat connexin40 gap junction channel is permeable to monovalent cations including tetramethylammonium and tetraethylammonium ions. Larger tetraalkyammonium (TAA^+) ions beginning with tetrabutylammonium (TBA^+) reduced KCl junctional currents disproportionately. Ionic blockade by tetrapentylammonium ($TPeA^+$) and tetrahexylammonium ($THxA^+$) ions were concentration- and voltage-dependent and occurred only when TAA^+ ions were on the same side as net K^+ efflux across the junction, indicative of block of the ionic permeation pathway. The voltage-dependent dissociation constants ($K_m(V_j)$) were lower for $THxA^+$ than $TPeA^+$, consistent with steric effects within the pore. The K_m–V_j relationships for $TPeA^+$ and $THxA^+$ were fit with different reaction rate models for a symmetrical (homotypic) connexin gap junction channel and were described by either a one- or two-site model that assumed each ion traversed the entire V_j field. Bilateral addition of $TPeA^+$ ions confirmed a common site of interaction within the pore that possessed identical $K_m(V_j)$ values for *cis–trans* concentrations of $TPeA^+$ ions as indicated by the modeled *I–V* relations and rapid channel block that precluded unitary current measurements. The TAA^+ block of K^+ currents and bilateral $TPeA^+$ interactions did not alter V_j-gating of Cx40 gap junctions. *N*-octyl-tributylammonium and -triethylammonium also blocked rCx40 channels with higher affinity and faster kinetics than TBA^+ or $TPeA^+$, indicative of a hydrophobic site within the pore near the site of block.

INTRODUCTION

Gap junction channels are unique among ion channels because they connect two intracellular compartments while traversing the extracellular environment. Hexamers of homomeric or heteromeric connexin subunits form a plasmalemmal transmembrane hemichannel that interacts with another hemichannel in a homotypic or heterotypic manner to form the intact gap junction channel. Gap junctions functionally integrate the coupled cells via electrical and chemical diffusion of ions and second messengers essential to tissue homeostasis and primary physiological function (e.g., excitation, secretion, contraction, transport). The ionic permeabilities of rat connexin-40, -43, -46, and *Xenopus* connexin38 (rCx40, rCx43, rCx46, and Cx38) homogeneous connexin hemichannel or gap junction channels, reveal quantitatively similar K^+/Cl^- permeabilities of $\cong$10/1 (Trexler et al., 1996; Beblo and Veenstra, 1997; Wang and Veenstra, 1997; Zhang et al., 1998). Furthermore, the relative permeability sequence for the group IA monovalent cations exhibited only minor deviations from their relative aqueous mobility sequence. These single salt ionic permeabilities and unitary channel conductances are the only information currently available about the ion-permeation pathway through connexin channels. Furthermore, although some three-dimension structure of hemichannels and gap junction channels are emerging, there are no direct structural correlates that define which protein domains line the transmembrane pore (Perkins et al., 1997, Unger et al., 1999).

Ionic affinities and interactions have always been integral to the development of mechanistic models for ion permeation through ion-selective channels. Structural correlates were obtained by combining mutational analysis with electrophysiological analysis of ionic conductance, permeability, or block of putative pore-forming sequences (French and Shoukimas, 1985; Yellen, 1987; Choi et al., 1993; Hille, 1992). For example, ionic blockade by tetraethylammonium (TEA^+) ions was instrumental in the identification of the signature pore segment of several voltage-dependent potassium channels (Armstrong and Binstock, 1965; MacKinnon and Yellen, 1990). Furthermore, TEA^+ and larger tetraalkylammonium cations, such as tetrabutylammonium (TBA^+), tetrapentylammonium ($TPeA^+$), and tetrahexylammonium ($THxA^+$) ions, are known to block ion permeation through the ryanodine receptor, nicotinic acetylcholine receptor, neuronal chloride, and anthrax toxin channels (Sanchez and Blatz, 1995; Sanchez et al., 1986; Tinker et al., 1992; Blaustein and Finkelstein, 1990a,b; Blaustein et al., 1990). Previously, we observed lower single-channel conductance (γ_j) and ionic permeability ratios ($\gamma_{TAA/K}$ or $P_{TAA/K}$) in the rCx40 and rCx43 channels with 115 mM tetramethylammonium (TMA^+) and TEA^+ ions (in Cl^- salts; Beblo and Veenstra, 1997; Wang and Veenstra, 1997). The $\gamma_{TAA/K}$ or $P_{TAA/K}$ ratios also closely followed their relative monovalent cation aqueous mobilities. However, unilateral addition of 115 mM TBA^+ abolished rCx40 junctional currents (I_j) when the transjunctional potential (V_j) was positive on the tetraalkyammonium (TAA^+) side even

Received for publication 8 March 2001 and in final form 24 September 2001.

Address reprint requests to Richard D. Veenstra, Dept. of Pharmacology, SUNY Upstate Medical Univ., 750 E. Adams St., Syracuse, NY 13210. Tel: 315-464-5145; Fax: 315-464-8014; E-mail: veenstrr@mail.upstate.edu.

0006-3495/01/12/3253/22 $2.00

though I_j was observed when V_j was reversed (KCl side positive, Beblo and Veenstra, 1997). Prolonged exposure to 115 mM TBA^+ proved toxic to the cells. We have investigated the actions of larger TAA^+ ions on the macroscopic junctional conductance (g_j) of rCx40 gap junctions by unilateral addition of millimole amounts of TBA^+, $TPeA^+$, and $THxA^+$ ions. We demonstrate, for the first time, ionic blockade of a homotypic connexin gap junction channel by large TAA^+ ions in a concentration- and voltage-dependent manner. Furthermore, we have modeled the voltage-dependent dissociation constants $K_m(V_j)$ for $TPeA^+$ and $THxA^+$ block of the rCx40 channel. The one- and two-site models both predict that $TPeA^+$ and $THxA^+$ permeate through the rCx40 pore. Bilateral addition of $TPeA^+$ reduced ionic blockade in exact proportion to the unilateral $K_m(V_j)$ for the opposite side [$TPeA^+$], consistent with single-site interactions between two $TPeA^+$ ions acting with identical binding affinities. Finally, we demonstrate that the addition of an octyl side chain increases the affinity and kinetics for block.

MATERIALS AND METHODS

Electrophysiological recording

Stable rCx40 transfected neuro2A (N2A) cell cultures were prepared and maintained as previously described (Beblo et al., 1995). N2A cell cultures were washed 3–5 times with HEPES-buffered saline immediately prior to use and placed on the stage of an inverted phase contrast microscope (Olympus IMT-2, Lake Success, NY). The bath saline contained (in mM): 142 NaCl, 1.3 KCl, 0.8 $MgSO_4$, 0.9 NaH_2PO_4, 1.8 $CaCl_2$, 4.0 CsCl, 2.0 TEACl, 5.5 dextrose, 10 HEPES, pH 7.4 (titrated with 1 N NaOH), 310 mosm. All junctional current recordings were performed using conventional double whole cell recording techniques using two Biologic RK-300 (Claix, France) or Axopatch 1D (Axon Instruments, Foster City, CA) patch clamp amplifiers (Veenstra and Brink, 1992; Beblo et al., 1995). Patch electrodes (PG52151-4, WPI, Inc., Sarasota, FL) had tip resistances of 4–6 MΩ prior to GΩ seal formation and patch break when filled with 140 mM KCl internal pipette solution (IPS). The standard KCl IPS contained (in mM): 140 KCl, 4.0 CsCl, 2.0 TEACl, 3.0 $CaCl_2$, 5.0 K_4BAPTA, 1.0 $MgCl_2$, 25 HEPES, pH 7.4 (titrated with 1 N KOH), 310 mosm. MgATP was added daily to achieve a final concentration of 3.0 mM. TAACl salts were added unilaterally as indicated for each experiment. TBACl, TPeACl, THxACl, and Tetraheptylammonium chloride (THepACl) were purchased from Aldrich Chemical (Milwaukee, WI) and stored as a 1-M stock solution in 18 MΩ-cm water or 70% ethanol and diluted as required with KCl IPS. The final osmolarity of the TAACl+KCl IPS was not adjusted because the maximum dose of 10 mM TPeACl altered the final IPS volume by 1% and the total osmolarity by 6%. For most [TAA^+], the IPS osmolarity was altered by ≈3%. All experiments were performed at room temperature (20–22°C). Off-line current and voltage data recordings were stored on VCR tape using a Neurocorder DR-484 2/4 channel digitizer (Cygnus Technology, Delaware Water Gap, PA) at 10 kHz direct from the patch clamp amplifier. All analyzed currents were digitized at 2 kHz and low-pass filtered at 100 Hz (WPI LPF-30) unless otherwise indicated. Analysis was performed using the DOSTAT analysis program (Manivannan et al., 1992). Final graphs and curve-fitting were performed using Kaleidagraph software (Synergy Software, Reading, PA).

To determine the magnitude of TAA^+ block, a voltage protocol was written that sequentially altered the holding potential (ΔV_1) of the TAACl + KCl-containing cell (cell 1) from negative to positive and back to negative potentials relative to the KCl-containing cell (cell 2) in 30-s intervals. The common holding potential (V_1 and V_2) was −40 mV for both cells. Cell 1 was stepped to this common potential for 1 s at the end of each 30-s voltage pulse and for 10 s between different −/+/− command voltages to assess any change in the nonjunctional voltage clamp circuit. $V_j = (V_1 + \Delta V_1) - V_2$ and ΔV_1 was altered in 5-mV increments from 10 to 50 mV and $I_j = -\Delta I_2$. One example of the I_j recordings obtained from an experiment with 10 mM TPeACl at $V_j = -/+/-40$ mV is shown in Fig. 1. There were no time-dependent changes in I_j observed during the control V_j pulse to −40 mV. Some time-dependent decay and recovery of I_j was observed during the first 5 s of the subsequent block and recovery ±40-mV V_j pulses in all TAA^+ experiments. I_j was averaged over the 29-s V_j pulse and junctional *I–V* relationships were plotted for every experiment as shown in Fig. 2. This plot demonstrates the reversibility of the TAA^+-dependent block using this voltage protocol. The maximum junctional conductance ($g_{j,max}$) was calculated from the slope of the linear regression fit of the −10 to −30-mV I_j-V_j curve for each experiment.

Synthesis of octyl-tributylammonium

Solutions of triethylammonium and tributylammonium were refluxed with equimolar amounts of 1-bromoocatane for 48 h in acetonitrile under an inert atmosphere (Halpern et al., 1982). The reaction mixtures were concentrated in vacuo, dissolved in water, extracted with ether, decolorized with activated charcoal, and lyophilized. All alkyl reagents were purchased from Aldrich Chemical. The chemical structures were confirmed by NMR spectroscopy. Stock solutions of 0.5 M *N*-octyl-triethylammonium (TEOA) and *N*-octyl-tributylammonium (TBOA) bromide were kept at −20°C until the day of use.

RESULTS

Concentration-dependence of TAA block

We first attempted to determine the magnitude and concentration-dependence of TBACl block of the rCx40 channel because the lack of I_j was first observed when this compound was added unilaterally at 115 mM to rCx40 N2A cells (Beblo and Veenstra, 1997). Stable I_j recordings were limited to ≤20 mM TBA^+ added unilaterally because the input resistance of the TAA^+-containing cell diminished over time. V_j-dependent gating was observed to commence at ≥±40 mV, consistent with the previous observations of Beblo et al. (1995). Because the analysis of voltage-dependent ionic blockade of an ion channel is best performed under conditions of constant (equal) open probability ($\mathbf{P}_o$), all quantitative analysis of ionic blockade was limited to the linear portion of the junctional *I–V* relationship for each experiment (i.e., $N \times P_o$ = constant). Reversible ionic blockade of I_j by unilateral TBA^+ at $V_j = +35$ or +40 mV was ≈10% of control I_j at 1 or 2 mM TBA^+ and achieved a maximum of ≈40% with 10 or 20 mM TBA^+ (Fig. 3 *A*). The reduction in I_j was even more pronounced at higher voltages where V_j-dependent gating is also more prevalent. The average g_j was 1.36 ± 0.56 nS ($n = 3$) for 1 mM TBACl, 5.02 ± 2.69 nS ($n = 3$) for 2 mM TBACl, 4.61 nS ($n = 1$) for 5 mM TBACl, 2.05 ± 1.58 nS ($n = 5$) for 10 mM TBACl, and 3.35 ± 2.24 nS ($n = 4$) for 20 mM TBACl. The average g_j was 2.96 ± 2.13 nS ($n = 16$) for all TBACl experiments, which was not statistically different

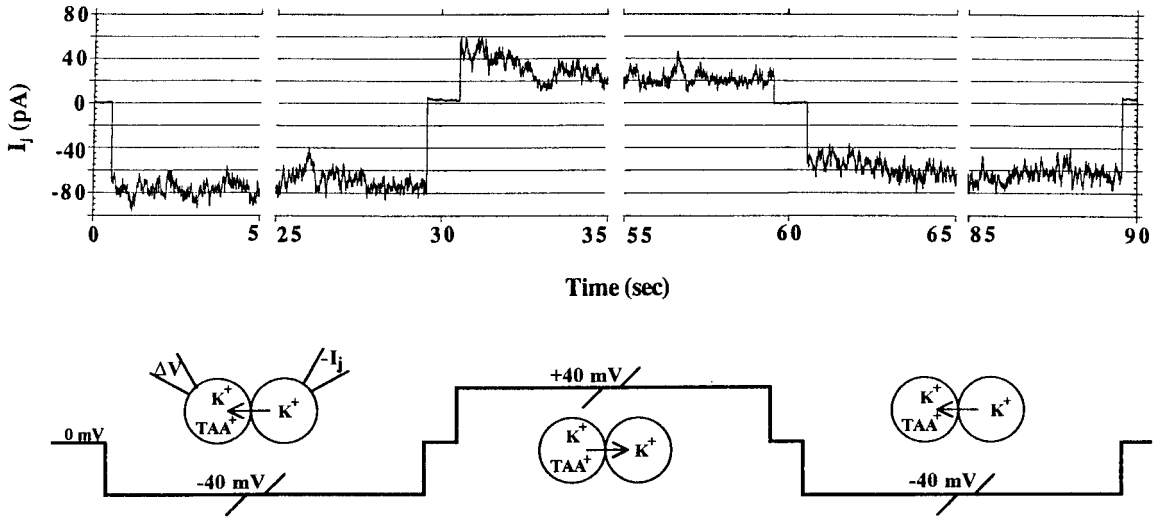

FIGURE 1 Whole cell currents from the postjunctional cell (cell 2) of a rat Cx40-transfected N2A (rCx40) cell pair demonstrating voltage-dependent block of junctional currents (I_j) in the presence of 10 mM tetrapentylammonium chloride. Shown is an excerpt from a single experiment displaying initial and steady-state currents elicited by a transjunctional voltage step (V_j) of ±40 mV. This is one sequence of an entire protocol in which V_j is varied in 5-mV increments from ±10 to ±50 mV. Voltage polarity is in reference to the prejunctional cell (cell 1). $TPeA^+$ ions were added only to the prejunctional cell (cell 1). For each V_j, cell 1 is stepped to a negative holding potential (negative V_j polarity, control) for 30 s, followed by a voltage step of equal amplitude and opposite polarity (positive V_j, block) for 30 s, and then returning to the control voltage for 30 s (recovery). Each 30-s step terminates with a 1-s interval where $V_j = 0$ mV. The common holding potential for both cells when $V_j = 0$ mV was −40 mV. Each +/−/+ voltage sequence is followed by a 10-s rest period ($V_j = 0$ mV). There is a significant reduction in I_j when V_j pulses of positive polarity are applied to cell 1 relative to steady-state currents obtained by the preceding and subsequent V_j pulses of negative polarity.

from previous observations of g_j with this clone of rCx40-transfected N2A cells (Beblo et al., 1995). Due to the limited V_j and TBA^+ concentration ranges where partial block of rCx40 g_j were observed in Fig. 3, no further analysis with TBACl was attempted.

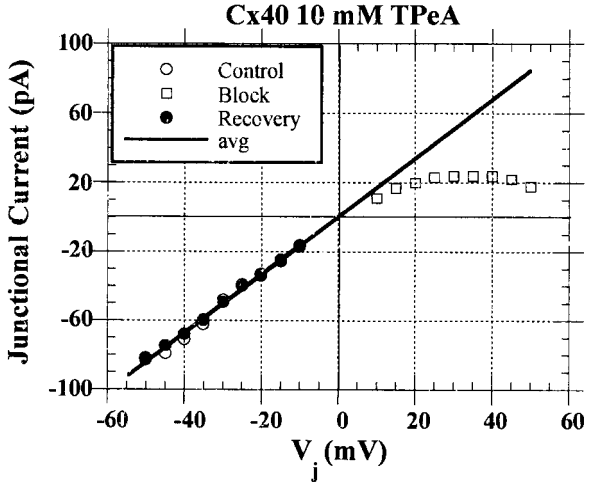

FIGURE 2 Whole cell junctional current–voltage (*I–V*) relationship from the same 10 mM $TPeA^+$ experiment shown in Fig. 1. The junctional *I–V* curve illustrates a reversible V_j-dependent and time-dependent block of rCx40 I_j at positive values that drive positively charged $TPeA^+$ ions into the pore.

The next largest TAA^+ ion in the series was $TPeA^+$, and the same experimental protocols were applied to the concentration-dependent block of rCx40 g_j. The upper limit that could be tolerated in KCl IPS with this compound was 10 mM TPeACl. The mean junctional *I–V* relationships for several $TPeA^+$ concentrations are presented in Fig. 3 *B*. The mean g_j was 4.00 ± 1.29 nS for 100 μM TPeACl ($n = 3$), 5.34 ± 3.04 nS for 200 μM TPeACl ($n = 4$), 4.00 ± 0.40 nS for 350 μM TPeACl ($n = 3$), 4.40 ± 2.27 nS for 500 μM TPeACl ($n = 3$), 9.56 ± 0.34 nS for 1 mM TPeACl ($n = 3$), 1.36 ± 0.31 nS for 2 mM TPeACl ($n = 2$), 3.61 ± 3.02 nS for 3.5 mM TPeACl ($n = 5$), 2.68 ± 1.91 nS for 5 mM TPeACl ($n = 4$), and 1.37 ± 0.18 nS for 10 mM TPeACl ($n = 4$). The average g_j was 4.01 ± 2.85 nS ($n = 31$) for all TPeCl experiments. I_j was reversibly reduced in a V_j- and concentration-dependent manner at all positive V_j values, as indicated by the linear junctional *I–V* at negative V_j (average of control and recovery I_j values, see Fig. 2). The junctional *I–V* relationships for each $TPeA^+$ concentration were pooled after normalizing each experiment to its linear slope g_j. V_j-dependent gating was observed at ≥±45 mV in all experiments. I_j declined only when the holding potential was more positive in the $TPeA^+$-containing cell, indicative of ionic block of the KCl permeation pathway (Tinker et al., 1992). The magnitude of the apparent $TPeA^+$ block was significantly greater than with identical concentrations of TBA^+ and achieved a maximum percent block of 64% at +40 mV with 10 mM $TPeA^+$.

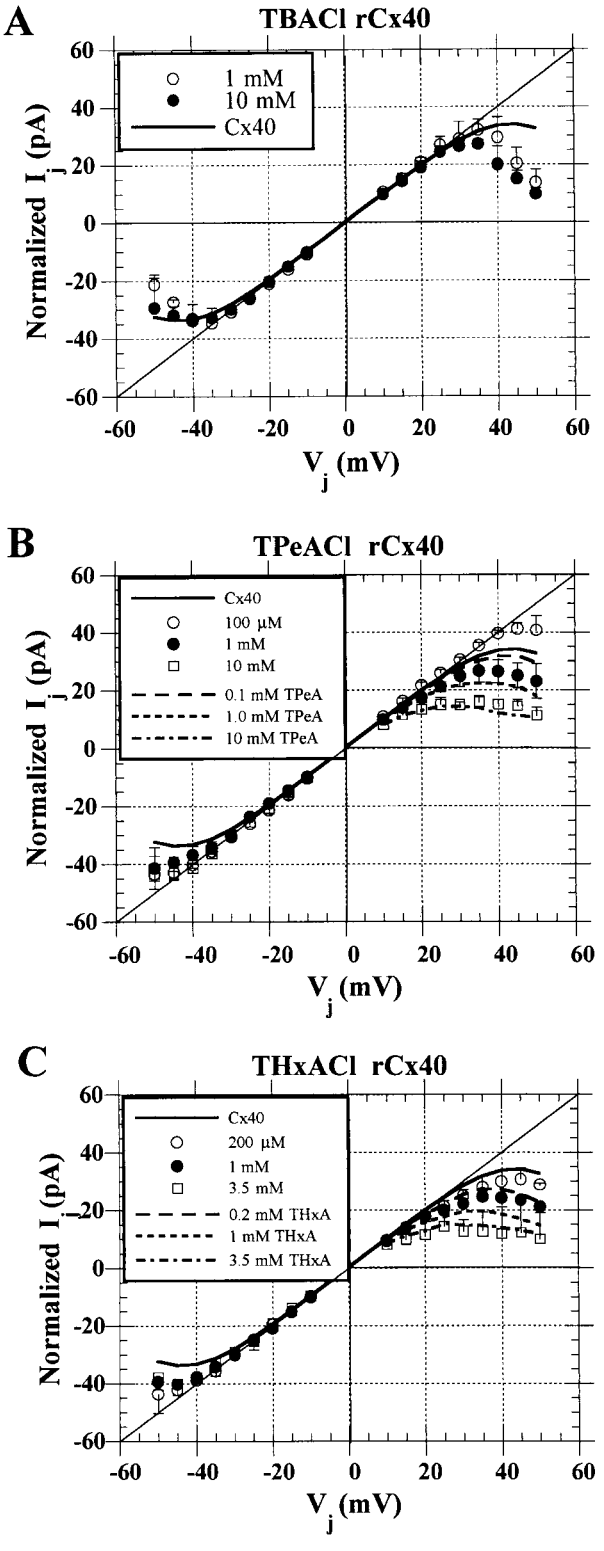

FIGURE 3 (*A*) Normalized steady-state junctional *I–V* curves for 1 mM TBA^+ ($n = 3$) and 10 mM TBA^+ ($n = 5$) added unilaterally to cell 1. Transjunctional voltage (V_j)-dependent closure is evident at $\geq \pm 35$ mV and additional block of I_j at $+V_j$ is due to the presence of 10 mM TBA^+. The solid line is the junctional *I–V* predicted for rCx40 gap junctions using Eq. 4 to predict the V_j-dependence of g_j as previously determined (Beblo et al., 1995, see text for details). Each experiment was normalized to the slope of the junctional *I–V* plot in the −10 to −30 mV range (linear range of V_j, see Beblo et al., 1995) and the normalized junctional *I–V*s were pooled for each [TBA^+]. Each data point represents the mean ± SD for each [TBA^+]. (*B*) Normalized steady-state junctional *I–V* curves for 100 μM ($n = 3$), 1 mM ($n = 3$), and 10 mM $TPeA^+$ ($n = 4$) added unilaterally to cell 1. The solid line again illustrates the V_j-dependent g_j for rCx40 according to Eq. 4, whereas the three different dashed lines indicated in the legend illustrate the additional effect of V_j-dependent block by 0.1, 1.0, and 10 mM $TPeA^+$ on rCx40 I_j according to Eq. 3. The $K_m(V_j)$ values for $TPeA^+$ are given in Table 1. All data for each [$TPeA^+$] were normalized as described for TBA^+. Each data point represents the mean ± SD for each [$TPeA^+$]. (*C*) Normalized steady-state junctional *I–V* curves for 10 μM ($n = 3$), 200 μM ($n = 3$), 1.0 mM ($n = 7$), and 3.5 mM $THxA^+$ ($n = 4$) added unilaterally to cell 1. The indicated lines again predict the junctional *I–V* according to Eq. 3 (various *dashed lines*) or Eq. 4 (*solid line*) using the $K_m(V_j)$ values for $THxA^+$ provided in Table 2. All data for each [$THxA^+$] were normalized as described for TBA^+. Each data point represents the mean ± SD for each [$THxA^+$].

$THxA^+$ was a more potent blocker than $TPeA^+$ as evidenced by the junctional *I–V* relationships illustrated in Fig. 3 *C*. The increasing hydrophobicity was also more evident because THxACl had to be dissolved in 70% ethanol to achieve a 1 M stock solution and was not tolerated internally at concentrations ≥5 mM in KCl IPS. Experimentally, the maximum degree of block actually observed with $THxA^+$ was the same as with $TPeA^+$ but it was achieved with only 3.5 mM THxACl in the KCl IPS. The mean g_j was 10.28 ± 3.13 nS for 10 μM THxACl ($n = 3$), 6.31 ± 2.25 nS for 35 μM THxACl ($n = 2$), 5.49 ± 1.88 nS for 50 μM THxACl ($n = 3$), 3.61 ± 2.16 nS for 100 μM THxACl ($n = 4$), 6.13 ± 0.44 nS for 200 μM THxACl ($n = 3$), 12.16 ± 6.80 nS for 350 μM THxACl ($n = 5$), 6.96 ± 6.19 nS for 500 μM THxACl ($n = 4$), 2.72 ± 1.87 nS for 1 mM THxACl ($n = 7$), 2.14 ± 0.84 nS for 2 mM THxACl ($n = 6$), and 1.47 ± 0.94 nS for 3.5 mM THxACl ($n = 4$). The mean g_j (5.34 ± 4.67 nS, $n = 41$) for all $THxA^+$ experiments was similar to the TPeACl g_j values. This demonstrates that the increasing amount of I_j blockade is a result of the addition of $THxA^+$ in place of $TPeA^+$ ions and not to differences in the I_j recordings. Furthermore, higher g_j values would lead to less observable I_j block because the series resistance error of the transjunctional voltage clamp increases with increasing g_j. The fraction of the applied V_j that actually drops across the junctional resistance (R_j) is proportional to the sum of the patch pipette resistances divided by the sum of both pipette resistances and R_j ($= 1/g_j$). This is true even when the whole cell patch electrode resistances are constant and ≤1% of the cellular input resistance. Hence, the data are consistent with the increasing effectiveness of progressively larger TAA^+ ions in producing I_j blockade.

Time-dependence of TAA block

The junctional *I–V* relationships displayed in Fig. 3, *A–C* were the mean steady-state junctional *I–V* relations for each [TAA^+] of the TBACl, TPeACl, and THxACl experiments performed. In some experiments, a similar voltage protocol was used to determine the magnitude of the time-dependent or time-independent (instantaneous) TAA^+ block and relief from block (unblock) with these organic cations. In these experiments, the 1-s rest interval at the common holding potential of −40 mV was omitted from the $-/+/-$ V_j sequence. The pulse duration was 30 s per pulse and the V_j increment was 5 mV. The net amount of instantaneous block and unblock observed upon $\mp$ and $\pm$ V_j polarity reversal results from the relative values of $k_{off}(V_j)/k_{on}$[TAA]. Analysis of the instantaneous and final I_j values of all block and recovery V_j pulses from 17 $TPeA^+$ (three 350-μM, one 500-μM, two 2-mM, four 3.5-mM, three 5.0-mM, and four 10-mM) and 27 $THxA^+$ (seven 350-μM, ten 500-μM, five 1-mM, three 2-mM, and two 3.5-mM) experiments did not reveal any instantaneous block of I_j by either compound at any [TAA^+] or V_j. Conversely, there was some instantaneous unblock that varied inversely with [TAA^+] and only slightly with V_j. Below 500 μM $TPeA^+$, the recovery from steady-state block was instantaneous at all V_j values. Figure 4 illustrates the amount of steady-state block of I_j that recovered instantaneously upon polarity reversal of V_j for 2 and 10 mM $TPeA^+$. The complete I_j traces from one 2-mM and one 10-mM $TPeA^+$ experiment at $-/+/-$ 40 mV are shown in panels *A* and *C*. The transitions from the steady-state block to the instantaneous recovery for these two experiments are displayed in panels *B* and *D*. The percentage of instantaneous unblock appeared to be concentration-dependent, decreasing from 51.3 ± 3.1% at 2 mM $TPeA^+$ to 22.2 ± 4.6% at 10 mM $TPeA^+$ for all V_j values examined (20–40 mV in 5-mV increments, panel *E*). Approximately 30% instantaneous unblock was observed for 3.5 and 5.0 mM $TPeA^+$. $THxA^+$ also exhibited a concentration-dependent instantaneous recovery from steady-state block. Instantaneous unblock at 350 μM $THxA^+$ appeared to be V_j-dependent, decreasing from 100% at 20 mV to 45% at 40 mV. This apparent V_j-dependent instantaneous relief of block was not evident at any of the higher [$THxA^+$] where <50% instantaneous unblock was observed for all V_j values (data not shown).

Because the entire steady-state block by both $TPeA^+$ and $THxA^+$ developed during the $+V_j$ pulse, the time-dependence of the decay phase of the I_j traces was fit with single- and double-exponential functions to determine the time constant(s) for steady-state block at each V_j. The difficulty with this analysis was that the magnitude of the steady-state block was typically only 2–4 times greater than the magnitude of the steady-state current fluctuations. This condition also applied to the (lower amplitude) time-dependent rising phase of the subsequent recovery (unblock) I_j traces. Therefore, the mean time constants and the experimental variability of the exponential fits were in excess of 100 ms for all [TAA^+] and V_j values. Individual fluctuations of I_j during a blocking or unblocking V_j pulse had time constants of <100 msec.

Voltage-dependent dissociation constants for TAA block

To determine the equilibrium constants for the blocking reaction, the fractional current ($I_{j,K+TAA}/I_{j,K}$) was plotted as a function of V_j for all concentrations of TPeACl and THxACl and fitted with the equation

$$\frac{I_{j,K+TAA}}{I_{j,K}} = \frac{1}{1 + ([TAA]/K_m(V_j))}. \quad (1)$$

Alternatively, the data were fit with the following expression, which assumes that complete blockade is never achieved

$$\frac{I_{j,K+TAA}}{I_{j,K}} = \frac{1 - I_{j,min}}{1 + ([TAA]/K_m(V_j))} + I_{j,min}. \quad (2)$$

The minimum unblocked fractional I_j ($I_{j,min}$) could result from partial blockade of the open rCx40 channel currents (i.e., a TAA^+-induced subconductance state), the inability to block a naturally occurring rCx40 subconductance state (i.e., a TAA^+-insensitive V_j-dependent subconductance state; $G_{j,min}$ = 0.30, Beblo et al., 1995), or a nonspecific background current that is insensitive to TAA^+-dependent block (i.e., a significant series resistance error in the junctional voltage clamp). The calculated $K_m(V_j)$ ± SD values for [$TPeA^+$] and [$THxA^+$] are summarized in Table 1. These estimated $K_m(V_j)$ values were used to fit the steady state junctional *I–V* relationships in Fig. 3, *B* and *C*, according to the expression

$$I_j = V_j \cdot \left[\frac{G_{j,max} - G_{j,min}}{1 + ([TAA]/K_m(V_j))} + G_{j,min}\right] \cdot \left[\frac{G_{j,max} \cdot [\exp(-0.12(V_j - 50)] + 0.30}{1 + [\exp(-0.12(V_j - 50)]}\right], \quad (3)$$

when $G_{j,max}$ = 1 (normalized slope conductance for each experiment) and $G_{j,min}$ is the estimated TAA-insensitive portion of $G_{j,max}$. The maximum junctional conductance ($g_{j,max}$) was determined from the slope of the linear regression fit of all *I–V* points between −10 and −30 mV for each experiment and $G_j = g_j/g_{j,max}$. The $g_{j,max}$ for all experiments averaged between 1 and 12 nS (see Results, Concentration-dependence of TAA block), and $G_{j,max}$ was defined to be 1. Normalized I_j equals $G_j \cdot V_j$ and the actual *I–V* curve is readily obtained by multiplying the normalized I_j values by $g_{j,max}$ for each experiment. Figure 3, *A–C*, is representative

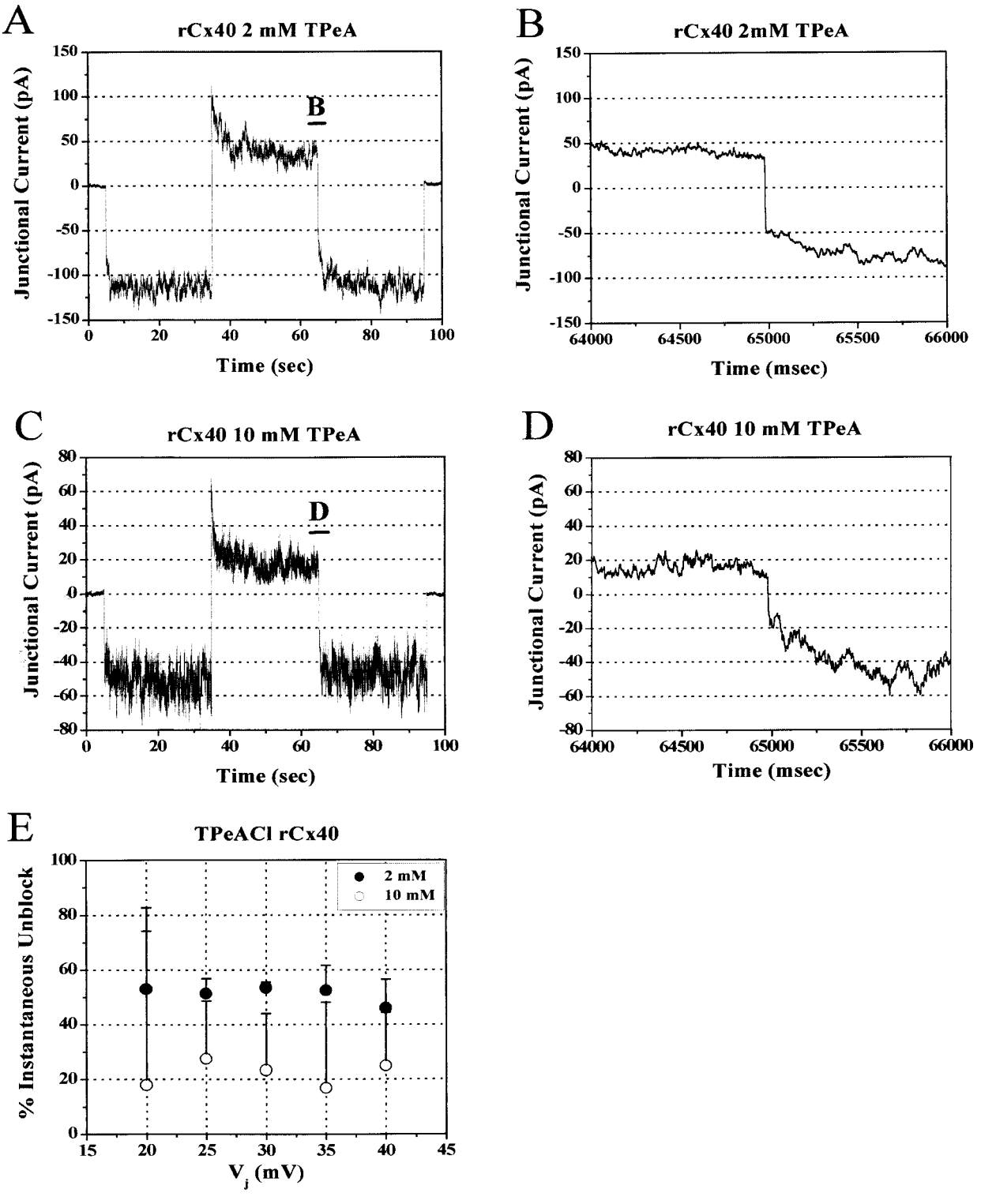

FIGURE 4 Instantaneous relief of block (unblock) upon $-/+$ V_j step to the indicated value for 2 mM and 10 mM $TPeA^+$. Instantaneous block during the $+/-$ V_j step was not observed for any [$TPeA^+$] as shown in panels *A* and *C* for 2 and 10 mM $TPeA^+$. The instantaneous relief of block by $TPeA^+$ decreased with increasing [$TPeA^+$] as observed in panels *B* and *D* from these same two experiments. The percentage (mean ± SD) of instantaneous block or unblock was calculated by dividing the change in instantaneous I_j by the difference in steady-state I_j for the control/block and block/recovery V_j steps (% instantaneous unblock = $[(\text{inst. } I_{j,\text{recovery}} - |\text{ss } I_{j,\text{block}}|)/(\text{ss } I_{j,\text{recovery}} - |\text{ss } I_{j,\text{block}}|)] \times 100$) for all 2 ($n = 2$) and 10 mM ($n = 4$) $TPeA^+$ experiments.

TABLE 1 Dissociation constants and minimum G_j for $TPeA^+$ and $THxA^+$ block of I_j

V_j (mV)	K_m + SE (μM)	$G_{j,min}$ ± SE	R
TPeACl			
+10	6019 ± 3885	0.66 ± 0.12	0.93
+15	3100 ± 1175	0.67 ± 0.05	0.97
+20	2738 ± 919	0.55 ± 0.06	0.97
+25	1572 ± 631	0.53 ± 0.06	0.95
+30	1384 ± 466	0.43 ± 0.06	0.96
+35	1130 ± 414	0.37 ± 0.07	0.95
+40	1058 ± 307	0.28 ± 0.06	0.97
+45	965 ± 246	0.26 ± 0.06	0.97
+50	601 ± 318	0.27 ± 0.10	0.87
THxACl			
+10	3836 ± 5692	0.64 ± 0.33	0.85
+15	2960 ± 2404	0.51 ± 0.23	0.92
+20	1374 ± 550	0.50 ± 0.09	0.96
+25	601 ± 219	0.55 ± 0.06	0.96
+30	868 ± 385	0.40 ± 0.11	0.94
+35	743 ± 278	0.34 ± 0.09	0.96
+40	473 ± 156	0.33 ± 0.08	0.95
+45	333 ± 97	0.32 ± 0.06	0.96
+50	250 ± 65	0.31 ± 0.05	0.97

pooled normalized I_j–V_j curves for the selected concentrations of TBA^+, $TPeA^+$, and $THxA^+$. The same procedures were applied to the bilateral $TPeA^+$ *I–V* curves (see Fig. 11), except that g_j was determined from the linear slope conductance between −10 and +10 mV of each experimental *I–V* curve because TAA^+ block is minimal at low V_j values. No $K_m(V_j)$ values were calculated for TBACl and the steady-state junctional *I–V* relationships in Fig. 3 *A* were fitted with the expression

$$I_j = V_j \cdot \left[\frac{G_{j,max} \cdot [\exp(-0.12(V_j - 50)] + 0.30}{1 + [\exp(-0.12(V_j - 50)]} \right], \quad (4)$$

that describes the predicted V_j-dependence of rCx40 from previous observations (Beblo et al., 1995). In Eqs. 3 and 4, $G_{j,max} = 1$ because all the experiments were normalized to their instantaneous slope conductances, 50 mV was the half-inactivation voltage (−50 mV for $-V_j$ values), and −0.12 (+0.12 for $-V_j$ values) was the slope factor of the Boltzmann curve that best described the V_j-dependent gating of g_j for rCx40. These data indicate that a concentration-dependent and V_j-dependent blocking mechanism can describe the nonlinear steady-state junctional *I–V* relationships observed in Fig. 3.

Complete block of I_j was not achieved within the experimental voltage range of ±50 mV, and the calculated fit of the experimental data with Eq. 2 provided a more accurate fit of the data because Eq. 1 requires that $I_j \rightarrow 0$. Examples of a few voltage-dependent dose–response curves for $TPeA^+$ and $THxA^+$ are shown in Fig. 5.

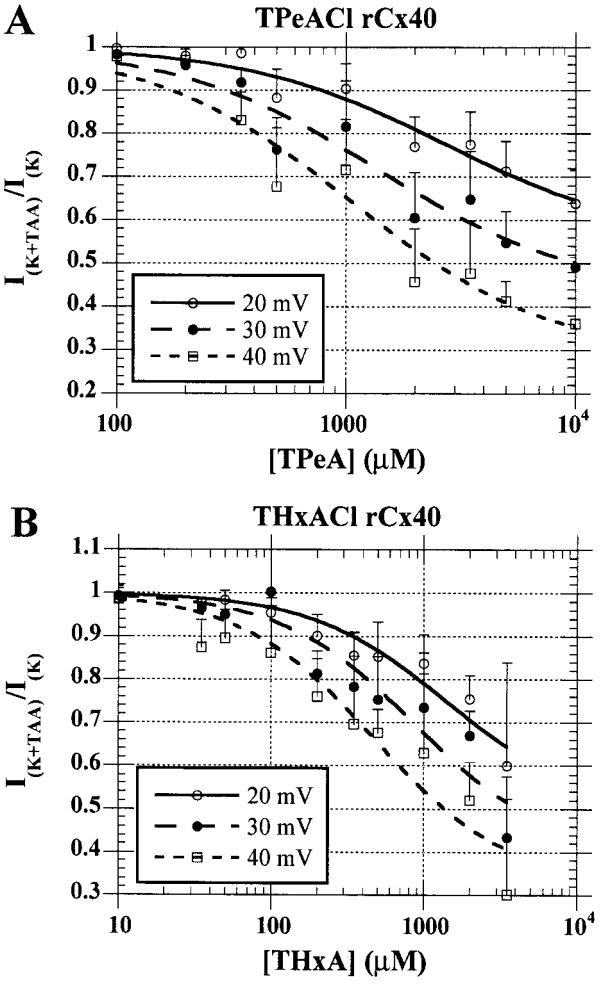

FIGURE 5 Dose–response curves for unilateral $TPeA^+$ and $THxA^+$ reduction of rCx40 I_j. The steady-state unblocked fraction of I_j was determined for each [TAA^+] and V_j by dividing the steady I_j at $+V_j$ by steady-state I_j at $-V_j$ (control and recovery pulses averaged together) for every independent experiment. Each data point is the mean ± SD for n experiments at each [TAA^+]. (*A*) Dose–response curves for $TPeA^+$ at the indicated V_j values. The curved lines are theoretical fits of the data using Eq. 2 (see text for details). The parameters of the fit are listed in Table 1. (*B*) Dose–response curves for $THxA^+$ at the indicated V_j values. The curved lines are theoretical fits of the data using Eq. 2 (see text for details). The parameters of the fit are listed in Table 1.

Barrier models for TAA block of the rCx40 channel

Since Woodhull (1973) derived a barrier model for voltage-dependent ionic block, voltage-dependent K_m have determined the relative energy profile of ion channels at the site of block by determining the fraction (δ) of the applied transmembrane voltage field sensed by the ions. That original derivation was for an asymmetrical inside–outside membrane channel. In the case of a homotypic gap junction channel, we have a symmetrical inside–inside double-membrane channel where the permeant ions remain electrically isolated from the extracellular potential. Given that the

applied V_j will be across two identical halves of the rCx40 gap junction channel, two possibilities exist. There could be a single ionic binding site formed by both homotypic rCx40 hemichannels that could sense the entire applied V_j or that each hemichannel contains its own ion binding site which could sense a maximum of $V_j/2$ of the applied V_j. To determine which one of these models best describes the TAA^+-dependent block of the rCx40 gap junctions, we derived similar expressions to the original Woodhull derivation for a symmetrical single-site and symmetrical two-site permeation pathway with or without a central compartment into which an ion could dissociate. The energy profiles for these one-site and two-site models are illustrated in Fig. 6, *A–C*. The mathematical derivations are provided in the Appendix. The $K_m(V_j)$ values listed in Table 1 that lie within the range of experimental [TAA^+] for $TPeA^+$ and $THxA^+$ were fitted with each of the expressions derived in the Appendix that correspond to the original Woodhull model for a permeant or nonpermeant blocking ion, Eqs. A6 and A7, respectively, and Eq. A16, for a permeant blocking ion traversing a two-site, four-barrier model. Only the two-site, four-barrier model yields a different expression for block by TAA^+ ions under unilateral conditions (see Appendix). The fraction of V_j sensed by these monovalent cations at the site(s) of block were determined from these theoretical fits to the experimental $K_m(V_j)$ data presented in Fig. 7. The δ and relative kinetic rate constants (e.g., b_{-1}/b_1) for the fitted curves are listed in Table 2. If the blocking TAA^+ is impermeant, only Eq. A7 applies to all three models. Only the $K_m(V_j)$ values $20 \leq V_j \leq 40$ mV were used because the estimated $K_m(V_j)$ values for 10 and 15 mV were highly variable and near the upper experimental [TAA^+] limit. V_j-dependent gating of g_j also became increasingly prominent when $V_j \geq \pm 40$ mV. The original Woodhull derivation for an impermeant blocking ion (Eq. A7) predicts an electrical distance (δ) of ≥ 1. This implies that the ion traverses the entire V_j field across the homotypic rCx40 gap junction channel. When we use the more appropriate Woodhull expression for a slightly permeant blocking ion (Eqs. A6), we obtain $\delta \approx 1.7$. This implies that, as soon as we permit TAA^+ ions to be on both sides of the blocking site, more than one ion (TAA^+ or K^+) occupies the pore. If two sites were included within the pore, one associated with each rCx40 hemichannel, a $\delta \approx 2$ is obtained. This again implies one permeant ion per site. Due to the high variability in the experimental K_m values and the predicted small differences between the one- and two-site models, the available experimental data unfortunately cannot distinguish between the one-site and two-site models. One test of whether each side of the channel has identical $K_m(V_j)$ values for the larger TAA^+ and how they might interact requires bilateral addition of TAA^+ ions. The data from two sets of bilateral $TPeA^+$ experiments are presented in the Results section.

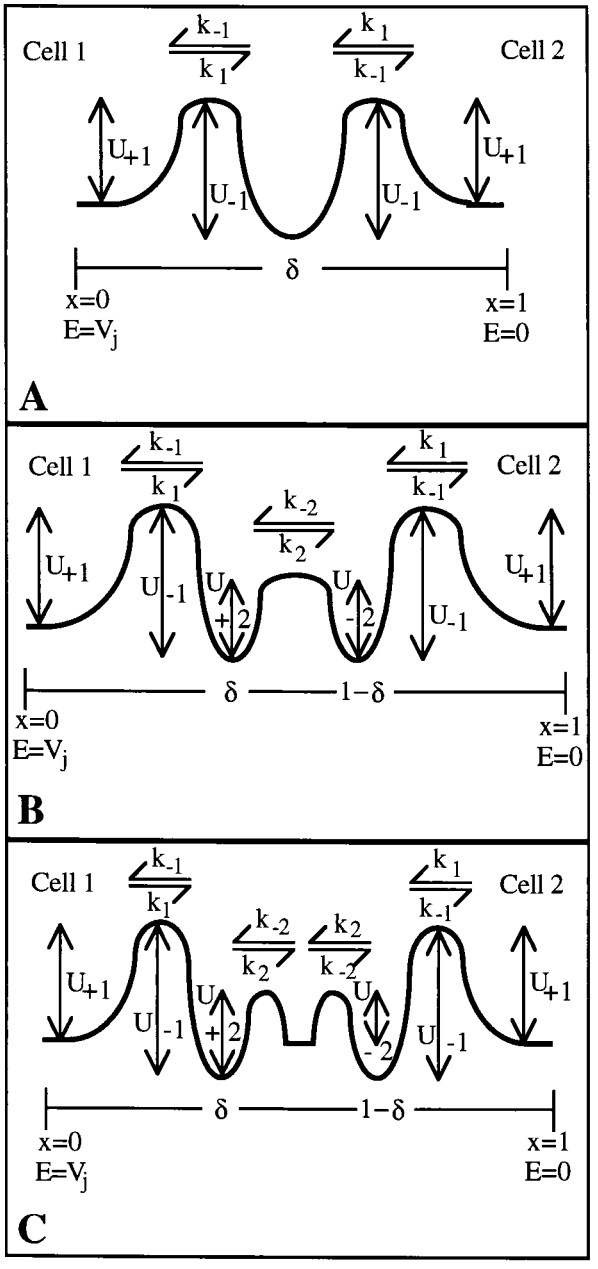

FIGURE 6 Model energy barrier diagrams for a symmetrical one-site (*A*) and two-site three- (*B*) or four-barrier (*C*) ion channel. Derivations for the voltage-dependent equilibrium dissociation constant ($K_m(V_j)$) appear in the Appendix according to the association and dissociation rate constants (e.g. $k_{1 \text{ or } -1}$) indicated in the diagram.

Single-channel analysis of TAA block of the rCx40 channel

All of the experiments presented in Figs. 2–5 and 7 were obtained from macroscopic conductance data from rCx40 N2A cell pairs. On occasion, single-channel currents were observed due to a lower g_j of <1 nS and different V_j protocols were performed to obtain unitary channel conductance (γ_j) and open probability (P_o) data from these mul-

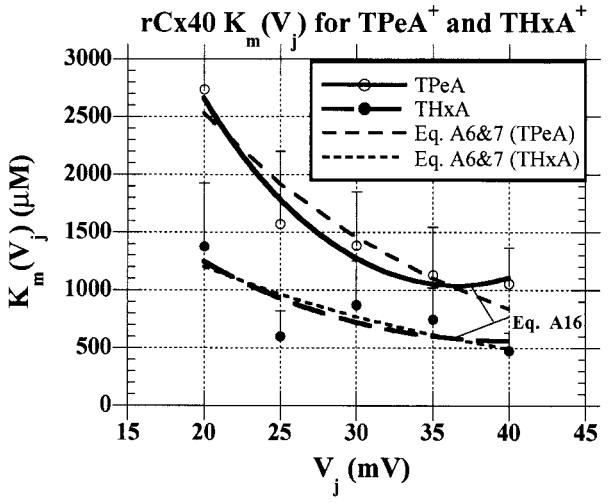

FIGURE 7 Theoretical fits of the V_j-dependent K_m values for $TPeA^+$ and $THxA^+$. The $K_m(V_j)$ values provided in Tables 1 and 2 over the +20- to +40-mV range were fitted with equations A6, A7, and A16 (see Appendix). Eqs. A6 and A7 represent the Woodhull (1973) derivation for a permeant and impermeant blocking ion with the exception that the channel is assumed to be symmetrical. Eq. A16 predicts the $K_m(V_j)$ values for a symmetrical channel with two ion binding sites. $TPeA^+$ and $THxA^+$ are also assumed to be permeant for Eq. A16. The estimated electrical distance (δ) and relative kinetic rate parameters from the fitted lines are listed in Table 2.

tichannel records. One experiment each with 2 mM $TPeA^+$ and $THxA^+$ are shown in Figs. 8 and 9. Both examples demonstrate a reversible reduction in P_o when V_j is positive with respect to the TAA^+-containing cell. These were the only two experiments that produced complete single-channel current–voltage relationships without the use of pharmacological uncoupling agents. Uncoupling agents such as octanol must be avoided because they also reduce P_o (Veenstra and DeHaan, 1988; Takens-Kwak et al., 1992). The junctional *I–V* relationships were also plotted for the current amplitudes observed in the all points histograms (panels *B*, *D*, and *F*) from both observed multichannel experiments (Fig. 10). The main state conductance of the rCx40 channel in the presence of $TPeA^+$ or $THxA^+$ was 150 ± 5.6 pS (n = 2). There were numerous rapid channel events observed in Figs. 8 and 9 that appear to be of reduced amplitude when filtered at 100 Hz and digitized at 2 kHz. These recording conditions have a temporal resolution of ≥6 ms for a full-amplitude event. Some of this data was resampled at 1 kHz low-pass bandwidth and digitized at 10 kHz to resolve these brief duration events with ≤1-ms resolution for full-amplitude events. There were no new peaks in the amplitude histograms to suggest the presence of a subconductance state of the rCx40 channel although the open channel noise did increase due to the wider recording bandwidth. Hence, the brief events observed in Figs. 8 *C* and 9 *C* during the $TPeA^+$ and $THxA^+$ blocking pulses achieve full amplitude openings and closings within the temporal resolution of the recording system.

Bilateral TAA as a test of the symmetry of block

If TAA^+ is added bilaterally, the steady-state junctional *I–V* should be predicted by using the $K_m(V_j)$ values already determined from unilateral addition of TAA^+, provided that TAA^+ entering the pore from either side binds and blocks independently of the *trans* side [TAA^+]. No interaction is expected to occur if two independent blocking sites exist or if a single blocking site is vacated prior to TAA^+ arriving from the opposite side upon V_j polarity reversal. The $TPeA^+$ and $THxA^+$ block and unblock data indicate that unblock is more rapid than block. Hence, bilateral addition of TAA^+ will not provide an accurate test of the one-site or two-site models unless interactions are observed between bilateral [TAA^+] as reported for voltage-gated potassium channels (Newland et al., 1992). To test this hypothesis, 500 μM $TPeA^+$ or 2 mM $TPeA^+$ was added to the *trans* side relative to 2 mM TPeACl. $TPeA^+$ was chosen because it was the more hydrophilic of the two blocking ions and 2 mM ≥ the experimentally observed $K_m(V_j)$ values (see Table 1). No interaction between *trans*/*cis* $TPeA^+$ ions is predicted by the 0.5/2 mM *I–V* curve (*long dashed line*) in Fig. 11 *A*. This result would indicate no apparent change in the $K_m(V_j)$ for either *trans* ($[TAA^+]_2$) 500 μM or *cis* ($[TAA^+]_1$) 2 mM $TPeA^+$, i.e., independent binding. Contrary to the unilateral block data, 500 μM *trans* $TPeA^+$ produced no block, and 2 mM *cis* $TPeA^+$ block was reduced from the unilateral condition (*trans* [$TPeA^+$] = 0). This phenomenon was observed before and after normalization of the three experimental *I–V* curves.

To model the observed shift in the *I–V* curve, we added the amount of I_j block expected from unilateral *trans* 500 μM $TPeA^+$ to the 2 mM *cis* $TPeA^+$ *I–V* curve. This theoretical result (Eq. 5 and Fig. 11 *A*, *short dashed line*) closely matched the experimental 500 μM/2 mM *I–V* curve (Fig. 11 *A*, *open circles* ± SD, N = 3). This result is

TABLE 2 Electrical distance (δ) estimates for $TPeA^+$ and $THxA^+$

Parameter	Eqs. A6	Eq. A7	Eq. A16	Eq. A6	Eq. A7	Eq. A16
δ	1.73 ± 0.31	1.41 ± 0.31	2.51 ± 0.39	1.45 ± 0.53	1.14 ± 0.53	1.97 ± 1.38
b_{-1}/b_1	3966 ± 798	7668 ± 2409	7615 ± 2663	1525 ± 848	2943 ± 1644	2291 ± 2814
b_2/b_1	NA	NA	3.7 ± 2.5	NA	NA	4.8 ± 8.8
R value	0.94	0.94	0.98	0.79	0.78	0.80

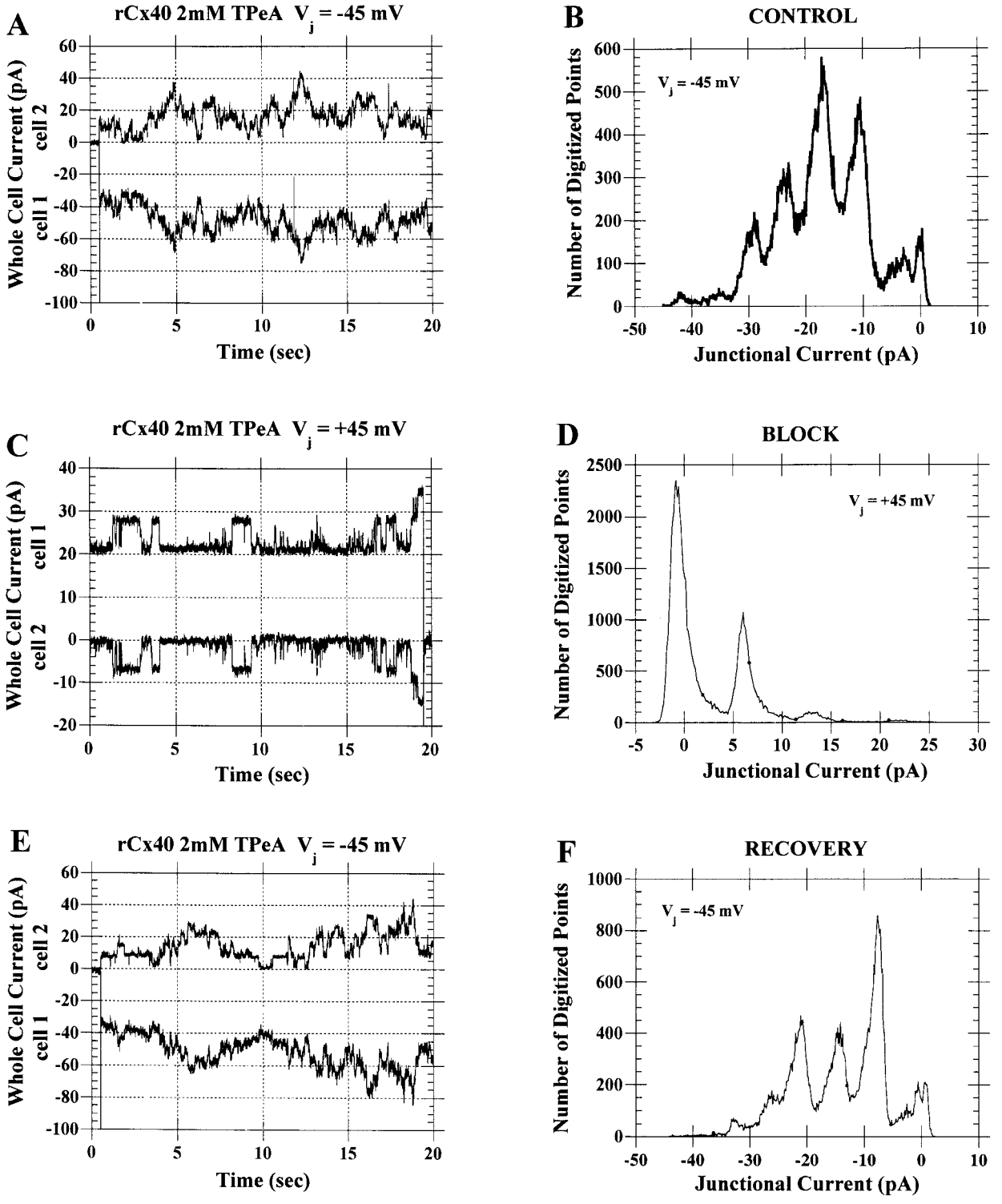

FIGURE 8 Blockade of rCx40 unitary channel currents by unilateral addition of 2 mM $TPeA^+$. Panels *A–F* are representative of a −/+/−45-mV V_j sequence obtained from a rCx40 cell pair with low g_j (≤1 nS). Panels *A*, *C*, and *E* illustrate all of the multichannel levels observed during each 30-s V_j pulse with IPS KCl in both pipettes and 2 mM $TPeA^+$ added only to cell 1. Panels *B*, *D*, and *F* are the all-points junctional current amplitude histogram for the entire 30-s V_j pulse. Six unitary channels are observed in the control (*A* and *B*) and recovery (*E* and *F*) −45-mV V_j pulses with $N = 1$ or 2 or 3 open channels being the predominant peaks accounting for 79% of the cumulative open time (cumulative open probability (P_o) = 0.79). Closed probability (P_c) was 0.06 excluding the 1-s $V_j = 0$ baseline interval during each −45-mV V_j pulse. During the +45-mV blocking pulse (*C* and *D*), P_c increased to 0.65 and the $N = 2$ or 3 open-channel peaks were nearly nonexistent ($P_o \leq 0.05$). Only the $N = 1$ open-channel peak is clearly evident in the histogram ($P_o = 0.27$), indicating that $TPeA^+$ blocked all six rCx40 channels ≈94% of the time as determined from a probability density function fit of the closed and $N = 1$ current peaks with $N = 6$ total channels. The unitary junctional current–voltage relationship is shown in Fig. 10.

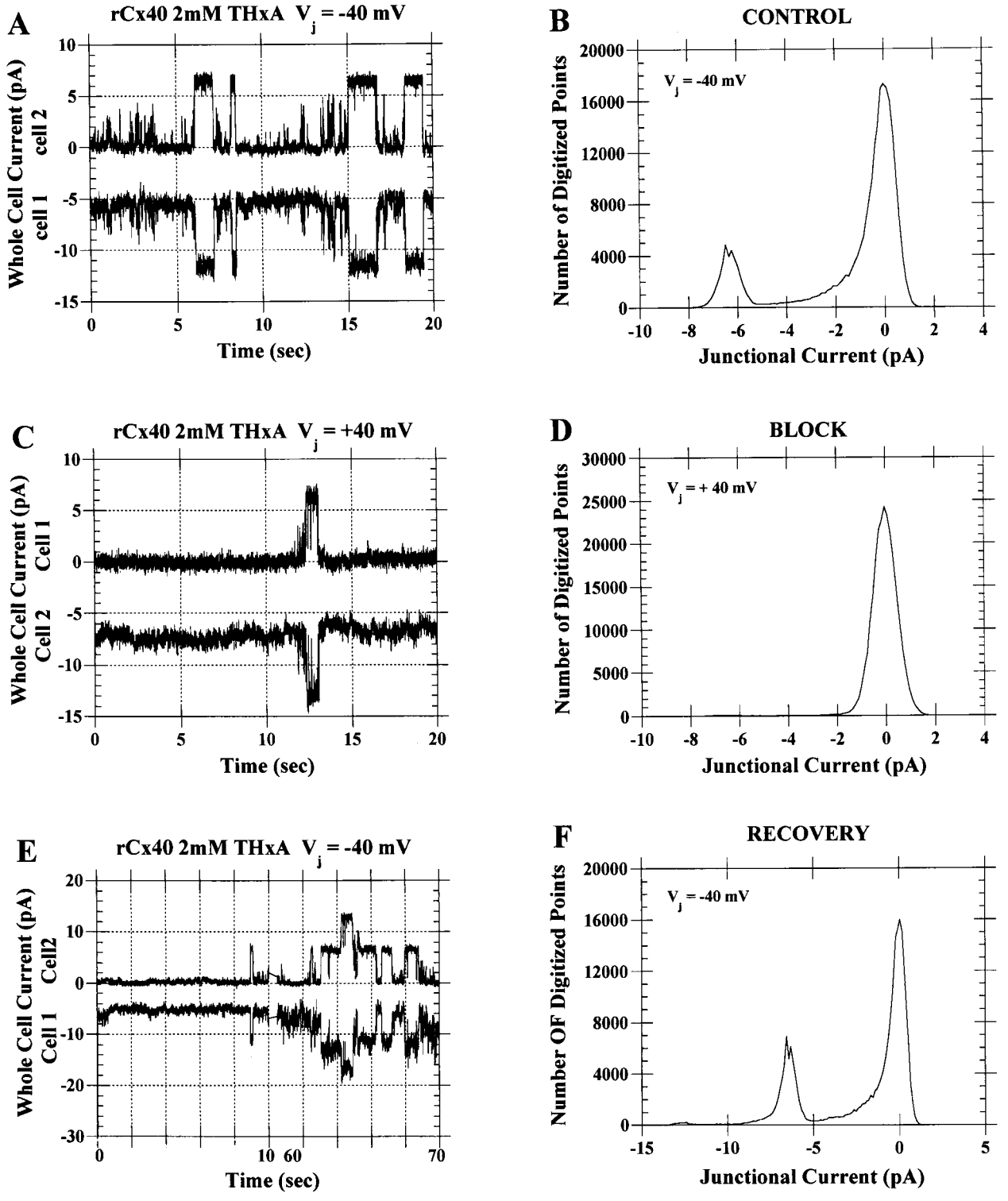

FIGURE 9 Blockade of rCx40 unitary channel currents by unilateral addition of 2 mM $THxA^+$. Panels *A*, *C*, and *E* are again representative current recordings that illustrate all of the open channel levels observed during each $-/+/-40$-mV V_j pulse. There was a maximum of $N = 2$ channels observed in this experiment. Each V_j pulse was 2 min in duration for this experiment and the $+V_j$ pulses were obtained by hyperpolarizing cell 2 by -40 mV in this example from a common holding potential of -40 mV for both cells. Panels *B*, *D*, and *F* are the junctional current amplitude histograms for each 2-min recording. The open probability for the $N = 1$ open-channel state was 0.15 for the control (panel *B*) and 0.23 for the recovery (panel *F*) pulses and <0.01 during the blocking V_j pulse (panel *D*). A second channel appeared only briefly during the entire 6-min recording (panels *E* and *F*, $P_o = 0.01$ for $N = 2$ state). The channel openings illustrated in panel *C* were the only observed channel events during the +40-mV V_j pulse. The unitary junctional current–voltage relationship is shown in Fig. 10.

expected if 500 μM $TPeA^+$ acting from the opposite side blocks I_j in exact proportion to the $K_m(V_j)$ values determined from the unilateral 500 μM $TPeA^+$ experiments (Figs. 3 *B*, 5 *A*, and Table 1). However, we can only estimate the amount of block by plotting $I_{j,K+[TAA]1}/I_{j,K+[TAA]2}$. For the unilateral case, $[TAA]_2 = 0$ (Eqs. 1 and 2). This model predicts that anytime $[TAA^+]_1 = [TAA^+]_2$, no net TAA^+ block will be observed because TAA^+ blocks I_j in identical proportion from either side of the channel. Furthermore, the intrinsic V_j-gating of rCx40 g_j is unaltered, thus indicating that $TPeA^+$ occupancy from one or both sides does not shift the V_j dependence of rCx40. Eq. 5 was obtained from Eq. 3 by adding the difference in g_j expected from the block produced by $[TAA^+]_2$ based on the unilateral K_m values.

$$I_j = V_j \cdot \left[\frac{G_{j,max} \cdot [\exp(-0.12(V_j - 50)] + 0.30}{1 + [\exp(-0.12(V_j - 50)]}\right] \cdot \left[\left[\frac{G_{j,max} - G_{j,min}}{1 + ([TAA]_1/K_m(V_j))} + G_{j,min}\right] + \left[\frac{(G_{j,max} - G_{j,min}) \cdot [TAA]_2}{K_m(V_j) + [TAA]_2}\right], \quad (5)$$

which reduces to Eq. 3 whenever $[TAA^+]_2 = 0$. This equation only applies when $[TAA^+]_1 \geq [TAA^+]_2$ because the general expression

$$\left[\frac{(G_{j,max} - G_{j,min}) \cdot [TAA]}{K_m(V_j) + [TAA]}\right]$$

defines the proportion of $G_{j,max}$ blocked by $[TAA^+]$, the general expression

$$\left[\frac{(G_{j,max} - G_{j,min}) \cdot K_m(V_j)}{K_m(V_j) + [TAA]}\right]$$

defines the proportion of $G_{j,max}$ not blocked by $[TAA^+]$, and

$$\left[\frac{(G_{j,max} - G_{j,min}) \cdot [TAA]}{K_m(V_j) + [TAA]}\right] + \left[\frac{(G_{j,max} - G_{j,min}) \cdot K_m(V_j)}{K_m(V_j) + [TAA]}\right] + G_{j,min} = G_{j,max} = 1.$$

Therefore, whenever $[TAA^+]_1 = [TAA^+]_2$, this expression reduces to Eq. 4.

This prediction was tested by two bilateral 2-mM $TPeA^+$ experiments. The results are illustrated in Fig. 11 *B*, where no $TPeA^+$ block of rCx40 g_j was observed in either direction, and the experimental data agree closely with the expected V_j-dependence of rCx40. These results are consistent with $TPeA^+$ binding with equal affinity from opposite sides of the channel and reducing the expected 2 mM *cis* $TPeA^+$ block by the precise amount expected from 500 μM or 2 mM *trans* $TPeA^+$ binding at an identical site at all V_j values. We do not know from macroscopic junctional *I–V* curves if g_j is already reduced proportionately by the respective *cis* and *trans* $[TPeA^+]$ because we cannot independently determine g_j in the absence of net cationic $K^+/TPeA^+$ flux depending upon the polarity of V_j as was performed under unilateral conditions. For the bilateral $TPeA^+$ experiments, g_j was normalized to the slope of the junctional *I–V* curve between -10 mV $< V_j <$ $+10$ mV where $TPeA^+$ block is minimal. The slope conductances were 0.80, 1.27, and 7.06 nS for the three 500 μM/2 mM $TPeA^+$ experiments and 4.48 and 5.31 nS for the two 2/2-mM $TPeA^+$ experiments.

These results are best explained by alternating occupancy by *cis* or *trans* $TPeA^+$ binding at one or more sites with a constant $K_m(V_j)$. The simplest explanation for multiple sites is the presence of two identical sites, although this model cannot definitively distinguish between two blocking ions interacting at one or two sites. A further test of the two-site hypothesis requires single-channel block data under bilateral conditions. Either rapid block occurs due to the alternating occupancy by *cis*/*trans* $TPeA^+$ or the channel open and closed dwell times are increased and reduced by *trans* $TPeA^+$ relative to the unilateral 2-mM $TPeA^+$ condition. Unfortunately, the latter case cannot be readily tested because gap-junction channel kinetics are too slow to acquire a reliable number of channel events to calculate the open and closed time distributions under unilateral and bilateral $TPeA^+$ conditions. The observation of only full-channel amplitude events, as occurred in the unilateral experiments,

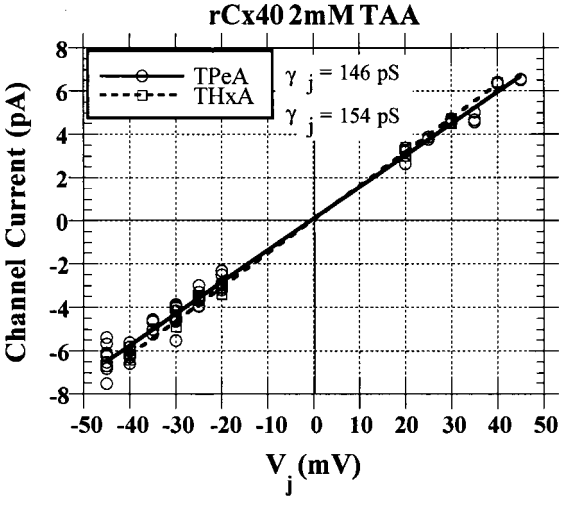

FIGURE 10 Single-channel junctional current–voltage relationships in the presence of either 2 mM $TPeA^+$ or $THxA^+$. The unitary amplitudes of the rCx40 channels present in the current amplitude histograms of Figs. 8 and 9 (panels *B*, *D*, and *F*) were plotted as a function of V_j, and a linear regression fit was performed on all of the data points for each experiment. The single-channel slope conductances (γ_j) were 146 and 154 pS for the open rCx40 channels in the presence of 2 mM $TPeA^+$ and $THxA^+$, respectively. These γ_j values are similar to the γ_j of 142 pS reported previously for the rCx40 in 115 mM KCl + 20 mM X^+ (12 Na^+, 8 Cs^+, and 3 TEA^+; Beblo and Veenstra, 1997).

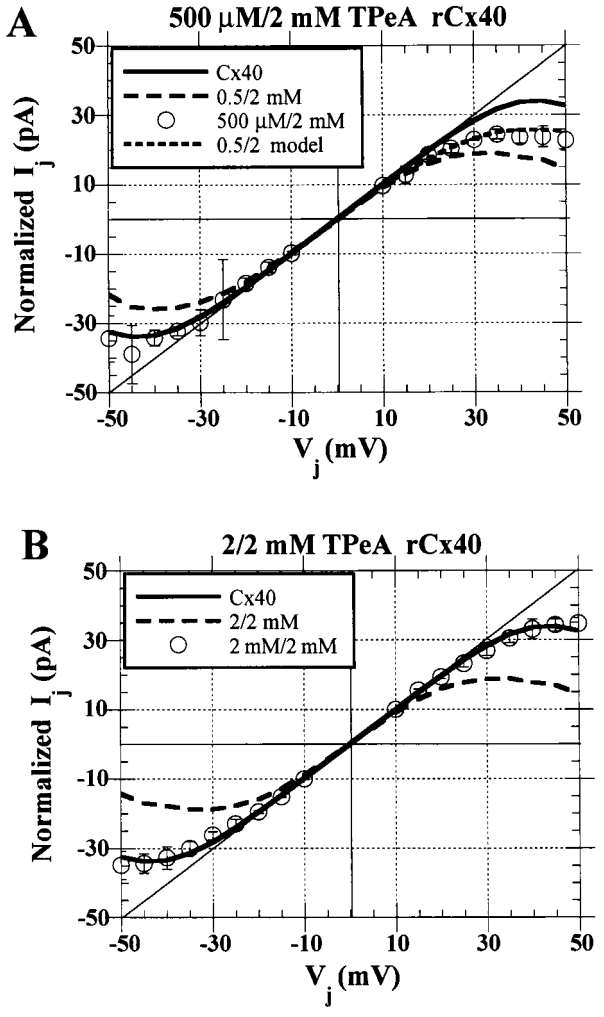

FIGURE 11 (*A*) Normalized steady-state junctional *I–V* curve for bilateral 500 μM/2 mM $TPeA^+$. The solid line is the junctional *I–V* predicted for rCx40 gap junctions using Eq. 4 (see text for details). The open circles represent the mean ± SD of three experiments on rCx40 gap junctions where 2 mM $TPeA^+$ was present in cell 1 (*cis*) with 500 μM $TPeA^+$ present in cell 2 (*trans*). Each experiment was normalized to the linear slope conductance of the *I–V* between −10 and +10 mV. The long dashed line (0.5/2 mM) illustrates the amount of block expected for unilateral addition of $TPeA^+$ at the respective concentrations. The short dashed line (0.5/2 model) was determined using Eq. 5 (see text for details) which predicts a reduction in the 2-mM *cis* $TPeA^+$ block in exact proportion to the expected block by 500-μM *trans* $TPeA^+$. (*B*) Normalized steady-state junctional *I–V* curve for bilateral 2/2 mM $TPeA^+$. The open circles represent the mean ± SD of two experiments on rCx40 gap junctions where 2 mM $TPeA^+$ was present in both cells 1 (*cis*) and 2 (*trans*). The long dashed line (2/2 mM) illustrates the amount of block expected for unilateral addition of $TPeA^+$ at the respective concentrations. No block is observed in either direction, consistent with Eq. 5 when equal concentrations of the blocking ion are present on both sides of the channel. Only the intrinsic V_j-gating of rCx40 is observed (Eq. 4) under these conditions.

or the observation of temporally unresolved flicker block of the rCx40 channel would favor the independent one-site model. The observation of full-amplitude channel events upon polarity reversal are indicative of the site(s) becoming unoccupied prior to block from the opposite side, a scenario most likely to occur with a single site. Rapid flicker or partial channel block (an apparent subconductance state) can result from simultaneous occupancy of one or two identical sites. Figure 12 demonstrates the continuous presence of flicker block under bilateral $TPeA^+$ conditions, consistent with *cis/trans* interactions at a single site.

Hydrophobic interactions at the site of block

Because the hydrophobicity of the TAA^+ ions increased with molecular size, we synthesized $TEOA^+$ and $TBOA^+$ ions to examine the effect of hydrophobicity on the block of Cx40 gap junctions. $TBOA^+$ possesses the same molecular mass as $TPeA^+$, however, the highest [$TBOA^+$] that was tolerated for the duration of the 15-min V_j protocol was 1 mM. Figure 13 illustrates that 1 mM $TBOA^+$ blocked only the V_j-sensitive component of I_j, but did so with faster kinetics than $TPeA^+$ (see Fig. 4). The amount of block is approximately equal to the block observed with TBA^+. The V_j pulse illustrated in panel *A* demonstrates the V_j-dependent gating of Cx40 during the −40-mV control and recovery pulses and the apparent lack of this V_j-gating during the +40-mV test pulse. Higher temporal resolution of the transition from the control to block V_j pulse reveals the rapid block by $TBOA^+$ to steady-state I_j values within 100 ms (panel *B*). A similar time course was revealed for the unblock of $TBOA^+$ from the steady-state I_j value to the full-peak value during the transition from the block to recovery V_j pulse (panel *C*). The normalized *I–V* curve from four 1-mM $TBOA^+$ experiments illustrates the rapid block of I_j by TBOA to control steady-state values.

$TEOA^+$ also produced V_j-dependent reductions in I_j at a concentration of 1 mM. In one macroscopic g_j experiment, the kinetics of block was slow, similar to that shown for $TPeA^+$ (data not shown). Two multichannel experiments further revealed a reduction in the open probability of the main Cx40 channel state with no reduction in channel current amplitude when $V_j \geq +30$ mV (data not shown). These results indicate that the mechanism of block is the same as that observed for $TPeA^+$ and $THxA^+$.

DISCUSSION

Ionic block of a gap junction

Ionic blockade has not been described for any gap-junction channel. The observation that TBA^+ did not carry current through rCx40 gap-junction channels (Beblo and Veenstra, 1997) led us to further examine the block of rCx40 gap junctions by larger TAA^+ ions. The results presented in this manuscript demonstrate that TBA^+, $TPeA^+$, and $THxA^+$ directionally reduce I_j in a manner that is fully reversible by changing the V_j polarity (Figs. 1 and 2). The direction of

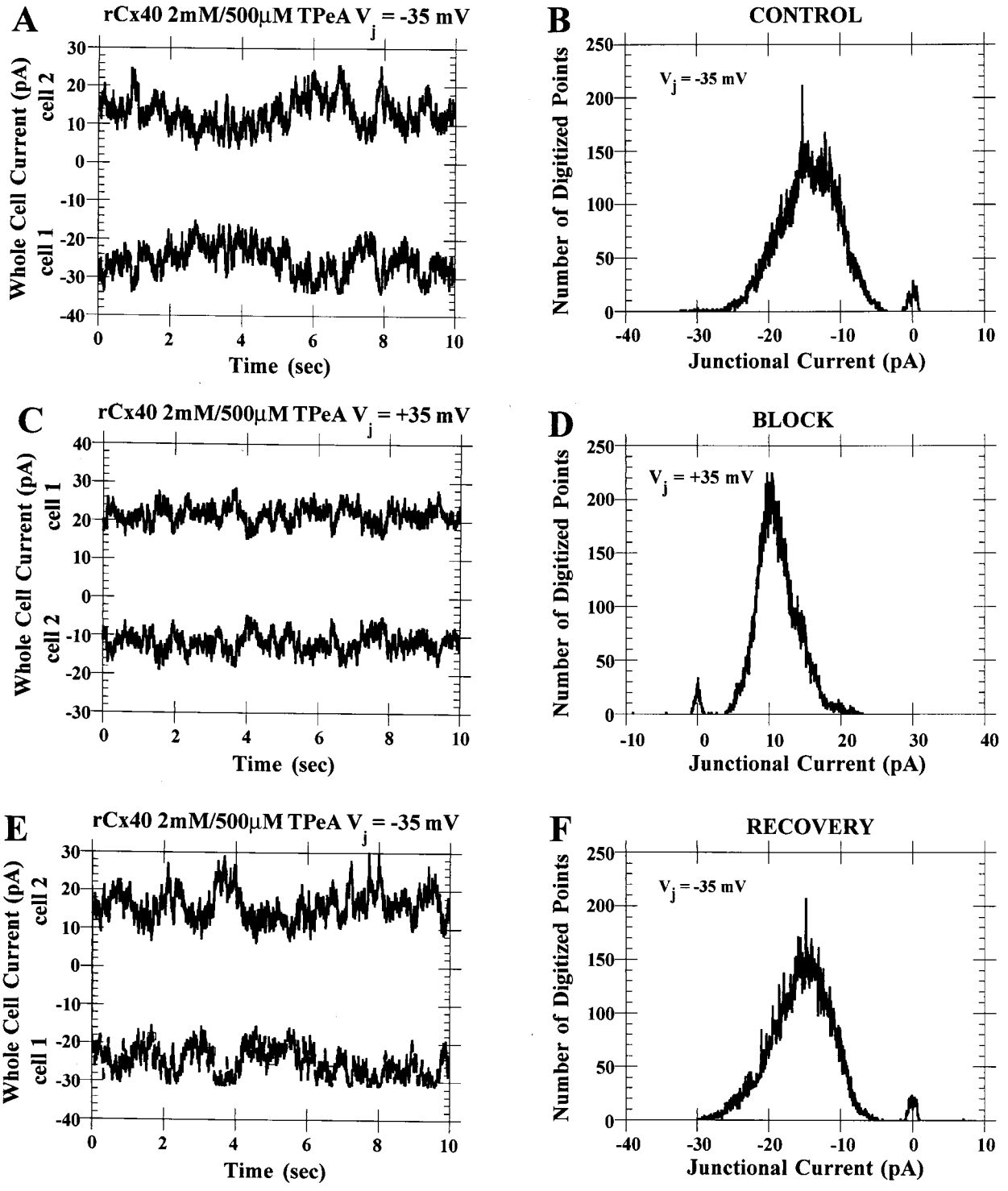

FIGURE 12 Blockade of rCx40 unitary channel currents by bilateral addition of 2-mM and 500-μM $TPeA^+$. Panels *A–F* are representative of a −/+/−35-mV V_j sequence obtained from a rCx40 cell pair with low g_j ($\leq$ 1 nS). Panels *A*, *C*, and *E* illustrate all of the multichannel levels observed during each 30-s V_j pulse with IPS KCl in both pipettes to which 2 mM $TPeA^+$ was added to cell 1 (*cis*) and 500 μM $TPeA^+$ was added to cell 2 (*trans*). Panels *B*, *D*, and *F* are the all-points junctional current amplitude histogram for the entire 30-s V_j pulse. Approximately four unitary channels are observed in the control (*A* and *B*) and recovery (*E* and *F*) −35-mV V_j pulses with $N = 1$ or 2 or 3 open channels being the predominant peaks. The open channels accounting for 100% of the cumulative recording time (cumulative open probability (P_o) = 1.0), excluding the 0.5-s $V_j = 0$ baseline interval during each −35-mV V_j pulse. During the +35-mV blocking pulse (*C* and *D*), the closed probability did not increase, and the $N = 1$ or 2 open-channel peaks were most prevalent ($P_o = 1.0$). All open and closed probability measurements were based on cumulative time distributions and no probability density function fits of the open-channel histograms with $N = 4$ total channels were attempted due to inability to resolve unitary channel current amplitudes.

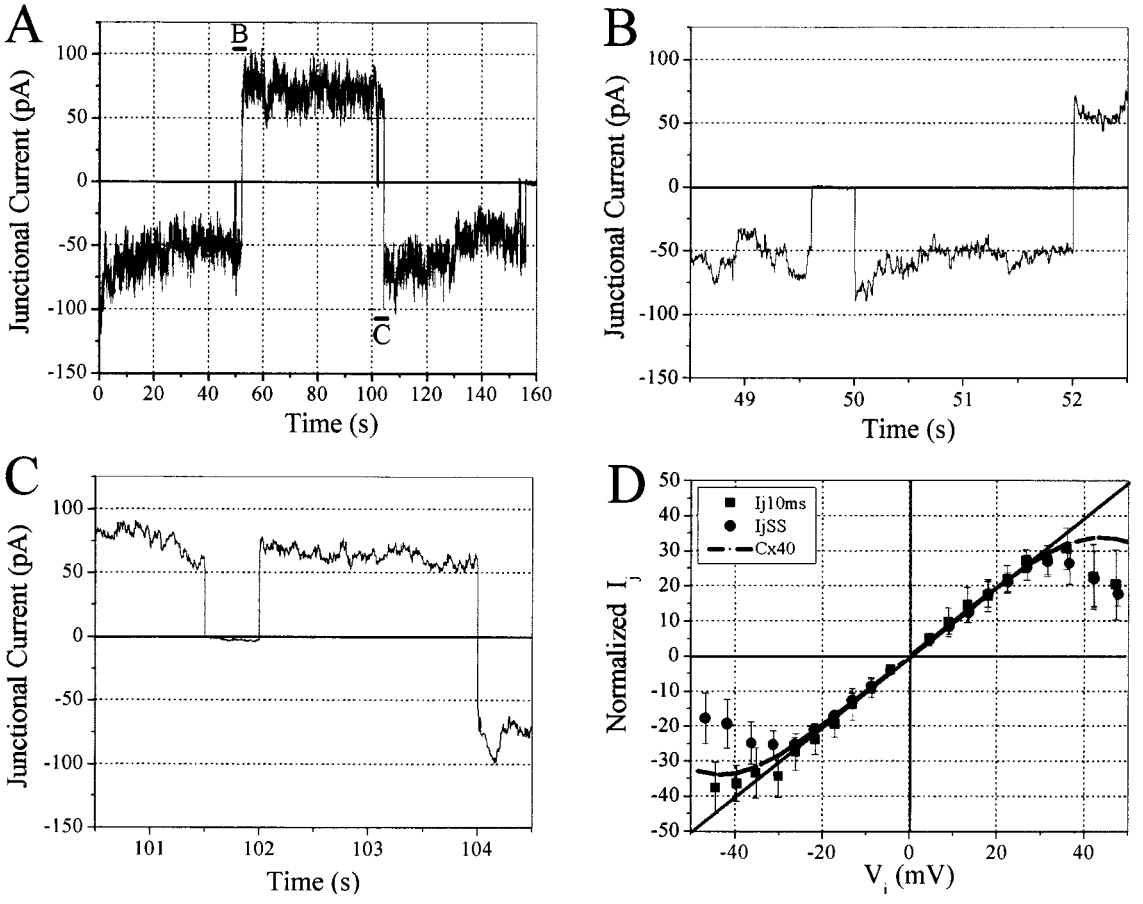

FIGURE 13 Increased kinetics of block by 1 mM $TBOA^+$. The complete 40-mV V_j protocol from one of four 1-mM $TBOA^+$ experiments illustrates the rapid block to steady-state levels of I_j (panel *A*). The control/block and block/recovery transitions are shown at higher temporal resolution in panels *B* and *C* as indicated. The normalized instantaneous (■) and steady-state (●) *I–V* curves for all four 1-mM $TBOA^+$ experiments are plotted in panel *D*. The mean value of I_j from 10 to 20 ms after the switch in V_j polarity was taken as the value of instantaneous I_j. The curved line depicts the V_j-dependence of Cx40 according to Eq. 4.

block was always in the direction of cationic current flow from the TAA^+-containing cell and was concentration-dependent (Fig. 3). Ionic blockade is also typically voltage-dependent (Woodhull, 1973). Our results demonstrate a decreasing K_m with increasing positive V_j (Fig. 5) for both $TPeA^+$ and $THxA^+$ in the rCx40 channel, consistent with this hypothesis. Because we are studying a double-membrane channel, we derived alternative expressions to the classical Woodhull equation for symmetrical (homomeric homotypic) and asymmetric (homomeric heterotypic) gap junctions, with V_j defined relative to the TAA^+-containing cell (Fig. 6 and Appendix). We obtained equivalent electrical distance (δ) values of ≥ 1 ion per site for both $TPeA^+$ and $THxA^+$ irrespective of the mathematical expression used to fit the data (Fig. 7). Mathematical descriptions reveal only minor differences between the one-site and two-site models that depend entirely on the V_j-dependent distribution of internal ions to produce any difference in the observed $K_m(V_j)$ values (Appendix). Multichannel recordings from low g_j rCx40 cell pairs revealed a V_j-dependent reduction in open probability without a reduction in the single-channel current amplitude (Figs. 8–10). Macroscopic g_j experiments revealed symmetrical block by $TPeA^+$ with identical $K_m(V_j)$ values to those determined from the unilateral experiments, indicative of a common site of interaction (Fig. 11). However, single-channel current recordings under bilateral $TPeA^+$ conditions revealed only "noisy" open-channel currents at all V_j values that made determination of γ_j impossible (Fig. 12). The unilateral application of 1 mM $TBOA^+$ and $TEOA^+$ also produced directional block resembling that of $TPeA^+$, thus revealing a role for a hydrophobic interaction in increasing the affinity for block (Fig. 13). The kinetics of $TBOA^+$ block was significantly faster than $TPeA^+$, despite their possessing identical chemical formula weights, suggestive of a further role of tethering the ion on the kinetics of block (Figs. 4 and 13).

Prior to these observations, all pharmacological blockade of g_j was produced by the external addition of amphipathic hydrocarbons (Johnston et al., 1980; Burt, 1989; Burt and Spray, 1989; Davidson and Baumgarten, 1988, Wu et al.,

1993; Guan et al., 1997). All of these amphipathic compounds are thought to act via partitioning into the biological phospholipid membrane, a mechanism consistent with the general anesthetic properties of the long chain alkyl alcohols, fatty acids, and halothane (Spray and Burt, 1990; Takens-Kwak et al., 1992; Bastiannse et al., 1993). Two of these uncoupling agents, octanol and heptanol, are known to act by reducing channel open probability (Veenstra and DeHaan, 1988; Takens-Kwak et al., 1992). This occurs in a voltage-independent manner and may involve deformations in the lipid bilayer–protein interface, resulting in altered channel conformations (Lundbæk and Andersen, 1999). The dependency of block on cationic current direction is not consistent with block by a lipophilic pathway, although hydrophobic TAA^+ interactions within a channel pore are known to occur (Armstrong, 1971; Choi et al., 1993). The organic TAA^+ ion series also possess hydrophobic properties that increase with the length of the substituted alkyl chains. Our observations with THepACl are similar to the results of Blaustein and Finkelstein (1990a) who found the analysis of voltage-dependent block of the anthrax toxin channel in planar lipid bilayers to be uninterpretable when using TAA^+ ions larger than $THxA^+$. It should be noted that they also used 10-fold less $TPeA^+$ to achieve voltage-dependent block than we had to use internally in live cell pairs. This initial analysis of TAA^+ block of the rCx40 channel provides new information about ionic permeation through homomeric homotypic connexin channels.

Mole fraction conductance–concentration curves and ionic blockade interactions have proven vital to the development of biophysical models for ionic permeation through specific channel pores. The purpose of examining the block by large TAA^+ ions was to explore the permeation pathway of gap-junction channels and possibly determine a definitive site for cationic block. Although we were not able to definitively identify the site of block by large TAA^+ ions, the observations provide much new information about the ion-permeation pathway of modestly cation-selective gap-junction channels.

Mechanism of block

Block of the permeation pathway of an ion channel is dependent upon the direction of permeant ion flow and concentration of the charged blocking molecule, and is characterized by voltage-dependent K_m values. $TPeA^+$ and $THxA^+$ exhibited all three of these properties. Because the rCx40 gap junction channel is symmetrical, there is no side specificity to the development of block. Apparent voltage-dependent block can occur by altering the gating of an ion channel or by occlusion of the conduction pathway. Blockade of ion conduction can occur by the plugging of the channel opening (gating type block) or by directly competing with permeable ions at a binding site along the conduction pathway (conduction or open-channel block) (Hurst et al., 1995). The former mechanism can occur whether the channel is open or closed and is time dependent whereas the latter mechanism occurs only when the channel is conducting and is quasi-instantaneous. Gap junctions are open at rest and close with prolonged V_j values $\geq V_{1/2}$ for inactivation of g_j. The V_j for rCx40 is ± 50 mV, which is why we did not use $V_{1/2}$ pulses in excess of ± 50 mV to examine the TAA^+ block of I_j. The V_j-gating of rCx40 appears to be unaltered in the junctional I–V curves (Figs. 3, 11, and 13), thus indicating that large TAA^+ ions occlude the ion conduction pathway. The voltage-dependent K_m values typically arise from a predominantly concentration-dependent on rate (k_{on}) and a predominantly voltage-dependent off rate (k_{off}) (Anderson et al., 1988; MacKinnon and Miller, 1988). Neither $TPeA^+$ or $THxA^+$ completely blocked I_j within the test V_j range, so the K_m values were determined for each test V_j assuming a finite TAA^+-insensitive conductance ($G_{j,min}$, Eq. 3). Incomplete block of ionic conductance was also observed with internal TEA^+, TBA^+, and $TPeA^+$ in the squid giant axon delayed rectifier K^+, the anthrax toxin, the sarcoplasmic reticulum Ca^{2+}-release, and the neuronal chloride channels (French and Shoukimas, 1985; Blaustein and Finkelstein, 1990a; Tinker et al., 1992; Sanchez and Blatz, 1995).

A nonzero G_{min} was also observed for the V_j-dependent inactivation of gap junctions and the G_{min} for rCx40 is 0.30 from uncorrected pulse protocol data and 0.25 from corrected continuous V_j ramp protocol data (Beblo et al., 1995; Veenstra, 2001). The G_{min} from the dose–response curves for $TPeA^+$ and $THxA^+$ was also 0.30 ± 0.03 (Fig. 5). This observation is consistent with the interpretation that the large TAA^+ ions cannot block the V_j-insensitive residual conductance of rCx40 that results from the formation of a subconductance state (Anumonwo et al., 2001). The same degree of block was also observed for $TEOA^+$ and $TBOA^+$, because I_j never decreased below steady-state I_j levels (Fig. 13). These observations suggest that large TAA^+ ions can block the main state of the rCx40 channel but not the residual subconductance state. $TPeA^+$, $THxA^+$, and $TEOA^+$ were all observed to completely block the main 155-pS conductance state without reductions in the single-channel current amplitude (Figs. 8–10). The observation of a reduced open probability due to the occurrence of prolonged blocked intervals is characteristic of toxin or gating type block of ion channels (Anderson et al., 1988; MacKinnon and Miller, 1988; Hurst et al., 1995).

Reductions in channel conductance are associated with rapid block–unblock events occurring within the ion permeation pathway (Hurst et al., 1995). TAA^+ ions produced this type of block in voltage-activated K^+ channels and the sarcoplasmic reticulum Ca^{2+}-release channels (MacKinnon and Yellen, 1990; Tinker et al., 1992). Contrary to these observed TAA^+-induced subconductance states, TAA^+ ions produced prolonged closed intervals without reductions in single-channel current amplitudes in the nicotinic acetyl-

choline receptor, the neuronal chloride, and the anthrax toxin channels (Sanchez et al., 1986; Blaustein et al. 1990; Sanchez and Blatz, 1995). The K_m for TBA^+ block of the anthrax toxin channel was 8 μM, the K_m for $TPeA^+$ block of the neuronal chloride was 80 μM, and the observed mean block intervals were $\cong$1 ms. Higher bandwidth recordings of the rCx40 channel did not reveal any rapid or partial block of the open-channel currents (low-pass bandwidth of 200 Hz or 1 kHz and digitization at 2 or 10 kHz). It was not possible to tell whether $TPeA^+$ and $THxA^+$ carried any junctional current below the 1-pA limit of whole-cell current recordings. The observed $K_m(V_j)$ values for the rCx40 channel were 10–100-fold larger than those previously observed values and the observed kinetics of block were also in the range of 100 ms to a few seconds in duration.

Instantaneous block of I_j was not observed with $TPeA^+$ or $THxA^+$, and instantaneous unblock was reduced by increasing $[TAA^+]$ (Fig. 4). The reduction in instantaneous unblock with increasing unilateral $[TAA^+]$ is consistent with a concentration-dependent k_{on} and voltage-dependent k_{off} rates for the rCx40 channel because the amount of unblock reflects the relative proportion of $k_{off}(-V_j)/k_{on}([TAA^+]_1)$. The amount of instantaneous unblock was also less with $THxA^+$ than with $TPeA^+$. These observations are consistent with a concentration-dependent k_{on} and voltage-dependent k_{off} and with slower off rates for TAA^+ ions of increasing size and hydrophobicity (Sanchez and Blatz, 1995). The blocking rate was postulated to be diffusion limited and based on the size of the ion relative to the pore (Blaustein and Finkelstein, 1990b). The neuronal chloride and anthrax toxin channels both have a finite permeability to counterions, as does the rCx40 channel (Beblo and Veenstra, 1997). The nicotinic acetylcholine receptor channel is relatively nonselective among monovalent cations, a property that was also observed for the rCx40 channel. The fastest rates of block were observed when we tethered TBA^+ to an octyl side chain to create the more hydrophobic $TBOA^+$ that has the same chemical formula weight as $TPeA^+$. The times required to achieve the maximum amount of block and unblock were nearly identical for $TBOA^+$ in contrast to the greater amount of instantaneous unblock observed with $TPeA^+$ (Figs. 4 and 13).

We were not able to determine the rates of block and unblock due to the slow channel kinetics and the low signal-to-noise ratio of the decay and recovery phases of I_j. Single gap-junction channel kinetics are much slower than most ion channels with open and closed dwell times of hundreds of milliseconds to seconds in duration (Figs. 8 and 9). This is consistent with our previous observations that 2-min pulses $\leq$50 mV produced fewer than 100 channel events for rCx43 or rCx40 (Beblo and Veenstra, 1997; Wang and Veenstra, 1997). The block that developed during 30-s $+V_j$ pulses did not remain constant for the duration of the pulse. These fluctuations in I_j may represent the dissociation and reassociation of $TPeA^+$ ions with the rCx40 channel at constant V_j values. This may be indicative of the low affinity of $TPeA^+$ for the rCx40 channel. We postulate that there is a low affinity site near the cytoplasmic entrance to the pore that $TPeA^+$ and $THxA^+$ ions readily dissociate from into the bulk solution in a V_j-dependent manner. The addition of a hydrophobic side chain restricts the location of the TAA^+ ion closer to the blocking site by associating with a hydrophobic site within the channel or at the membrane interface.

All observations of TAA^+ block of rCx40 are consistent with a gating type of open channel block where the blocking ion senses the entire V_j field. The bilateral $TPeA^+$ experiments prove that this block can develop from either side with equal affinity (Fig. 11). This observation is consistent with each side having an independent site and does not require the TAA^+ ion to be permeable. However, the channel data under bilateral conditions proved the existence of flicker block, indicative of rapid open-channel block within the permeation pathway (Hurst et al., 1995). That this flicker block was observed only under bilateral $TPeA^+$ conditions is consistent with rapid association–dissociation of bilateral $TPeA^+$ from a common site. The disappearance of prolonged blocked intervals was probably due to the increased $TPeA^+$ dissociation rate induced by $TPeA^+$ ions from the opposite side (knock-off). Destabilization of the blocked state can result in unresolved unitary channel currents. For example, the E395C mutation in the S4–S5 linker of the *Shaker* K^+ channel produced a rapid flickering channel that precluded unitary channel current measurements (Holmgren et al., 1996). The S4–S5 linker serves as the receptor for the *N*-terminal inactivation ball. Thus, we believe that $TPeA^+$ is permeable through the rCx40 channel and that block occurs within the ion permeation pathway.

The estimated diameters of TBA^+, $TPeA^+$, $THxA^+$ are approximately 9.5, 10.5, and 11.5 Å, respectively (Robinson and Stokes, 1965). Our estimate of the rCx40 pore diameter was 13.2 $\pm$ 1.4 Å. The 12–14-Å estimated range of the rCx40 pore diameter implies that there is a minimum of $\approx$2 Å and a maximum of $\approx$4 Å of free space between the walls of the pore when occupied by a $TPeA^+$ or $THxA^+$ ion. This leaves only enough space for a single water molecule or a completely dehydrated K^+ ion to occupy the remaining space. Given the weak cationic selectivity of the rCx40 channel, it seems unlikely that a K^+ ion would ever become completely dehydrated and transit past a $TPeA^+$ or $THxA^+$ ion occupying the pore at this site. The apparent $K_m(V_j)$ values for $TPeA^+$ and $THxA^+$ also decreased with increasing ion diameter and were nearly 100-fold less than the estimated K_m for KCl in the Cx40 gap junction channel (Veenstra and Wang, 1998). These observations favor the steric hindrance of KCl permeation when the connexin pore is occupied by TAA^+ ions.

The site of block

$TPeA^+$ and $THxA^+$ were observed to have V_j-dependent K_m values indicative of an ionic blocking mechanism. Woodhull (1973) demonstrated that one could determine the proportion of the applied voltage ($= z\delta$ V) sensed by all ions at the site of block. The determination of the voltage-dependent K_m and the electrical distance (δ) values provide two measurements of the ionic block that can assist in identifying the location of the blocking site. We attempted this analysis on the rCx40 gap junction channel with $TPeA^+$ and $THxA^+$ with the hope of providing a definitive measure of a putative monovalent cation binding site within the channel pore. Because the channel being studied is a symmetrical double membrane structure, we derived alternative two-site models to the original Woodhull (1973) derivation for an asymmetric, one-site channel in an attempt to further define whether one or two cation binding sites exist for a gap junction (Fig. 6 and Appendix). This analysis revealed that there are one or more ions per site whether the one- or two-site models were used to fit the data (Fig. 7 and Table 2). The variability in the δ values was proportional to the variance in the experimental K_m values for both compounds. However, a homomeric homotypic gap-junction channel presents a special case that requires further consideration. Because the cytoplasmic pore opening on either side of the channel is identical, this ion must be permeable if there is only a single site, because access to the site is identical from either side. This implies that, if TAA^+ is not permeable, there must be more than one blocking site. Hence, the estimate of electrical distance δ obtained with the analogous expression to the Woodhull derivation (Eq. A7) cannot apply to the homomeric homotypic connexin gap-junction channel unless there are identical sites on each side of the channel for the impermeant cation. Therefore, only the results with Eq. A6 or A16 are valid for the one- and two-site models, respectively. Because the value of δ depends on the fraction of the electrical field sensed by all of the ions in the pore, the variations between the internal ($1–2\delta$) or ($1–3\delta$) voltage-dependent terms from these one- and two-site derivations are expected to be minor (see Appendix). Thus, discriminating between a one- and two-site model for a poorly permeable blocking ion is virtually impossible. These derivations outline the experimental and biophysical conditions necessary to delineate between the one- and two-site models for homotypic and heterotypic gap-junction channels using this approach. In either case, the $z\delta$ value of ≥ 1 suggests that TAA^+ ions are permeable through the entire V_j field, and that there may be more than one ion per site.

One observation that demonstrates the permeability of a blocking ion is the relief of block at higher voltages that drive the blocking ion into and through the channel. Unfortunately, this was not demonstrated for the rCx40 channel due to V_j-dependent gating above ± 40 mV. The anthrax toxin, neuronal chloride, nicotinic acetylcholine receptor, and sarcoplasmic reticulum Ca^{2+}-release channels also produced $\delta \geq 1$ and incomplete current blockade (Blaustein et al., 1990; Sanchez et al., 1986; Sanchez and Blatz, 1995; Tinker et al., 1992). Our data are consistent with these prior observations with large TAA^+ ions. The slight variations between the one-site and two-site models and the knowledge that the Woodhull model does not apply to permeable blocking ions and multi-ion pores in the same manner as it does for complete channel blockade further defines the limitations of this approach (Yellen, 1987).

Two homomeric connexin hemichannels, Cx38 and Cx46, were demonstrated to have weak monovalent cation selectivities and nearly identical cation/anion permeability ratios of $\cong$10/1 (Trexler et al., 1996; Zhang et al., 1998). Similar cationic selectivities were observed in the intact rCx40 and rCx43 homomeric homotypic gap-junction channels (Beblo and Veenstra, 1997; Wang and Veenstra, 1997). On the basis of this data, we estimated the Cx46 and *Xenopus* Cx38 hemichannel pore diameters to be 11.0 ± 1.2 Å and 16.2 ± 2.0 Å relative to 13.2 ± 1.8 Å for Cx40 (Veenstra, 2000). If the steric hindrance mechanism of block is true, we predict that TBA^+, $TPeA^+$, and $THxA^+$ would be more effective blockers of the Cx46 channel, and the amphibian Cx38 channel would be less affected.

It seems likely that two hemichannels (an intrinsically asymmetrical channel analogous to the Woodhull model) with similar transmembrane architectures would link to form a continuous (symmetrical) channel wherein the gating and ionic selectivity properties are modified due to the imposed symmetry. The three-dimensional structures of the Cx32 hemichannel and truncated Cx43 gap junction channels both place the narrowest region of the homomeric and homotypic connexin pore near the extracellular membrane surface interface (Perkins et al., 1997; Unger et al., 1999). This observation suggests that hemichannel docking to the exclusion of the extracellular solution does not dramatically alter the transmembrane configuration of connexin channels. However, these crystallized gap-junction plaques likely represent an irreversible closed state of the gap junctions (Peracchia, 1977; Baldwin, 1979; Guan et al., 1997, Unger et al., 1999). It is difficult to reconcile strikingly similar ionic selectivities between homomeric connexin hemichannels and homomeric homotypic connexin gap-junction channels using a symmetrical single-site model. The simplest explanation is that each hemichannel possesses its own selectivity filter and gate.

Utility of TAA^+ block of gap junctions

The utility of intracellular large TAA^+ ions as a specific block of gap-junction channels is limited by their block of the sarcoplasmic reticulum calcium release, the neuronal chloride, and the delayed rectifier potassium channels (French and Shoukimas, 1985; Sanchez and Blatz, 1995;

Tinker et al., 1992). Despite their larger size, the electrical distance, δ, to the blocking site of the squid axon delayed rectifier K^+ channel by TBA^+ or $TPeA^+$ was the same as that of TEA^+. Preliminary results from this laboratory also indicate that $TPeA^+$ and $THxA^+$ block the rCx43 channel (Veenstra, 2000). Consequently, these large TAA^+ ions may not be useful for electrophysiological purposes on native cell types like cardiac myocytes, because many channel types will likely be affected even though they would be effective in lowering g_j.

CONCLUSIONS

We conclude that $TPeA^+$ and other large TAA^+ ions block KCl currents through the open rCx40 channel by completely occluding the channel from either side that involve both electrostatic and steric interactions within a narrow region ($\approx$12 Å) of the pore. A nearby hydrophobic site enhances the affinity and kinetics of block. The rapid dissociation under unilateral conditions indicates that the site is readily accessible from the cytoplasm. The shortened blocked intervals under bilateral conditions indicate that the site is accessible from both sides of the channel with equal affinity.

APPENDIX

Derivations for effective valence expressions of gap-junction channels

The transmembrane energy profile of any ion channel is represented by one or more binding sites ("energy wells") bounded by energy barriers of varying proportion in units of thermal energy ($-U_b/RT$). For the case of an ion moving in an electric field, there will be an additional energy component associated with the applied transmembrane voltage ($-zF\delta E/RT$) where δ is the fractional distance ($(x = 0) \le \delta \le (x = 1)$) traveled by the ion from bulk solution to the internal binding site. The product of $zF\delta E$ represents the effective valence of ions sensing the entire voltage E or the "fraction of the applied potential" E sensed by an ion of known valence z. For every energy barrier, the total energy difference for an ion to cross that barrier is given by

$$k_b = a_b \exp\left(\frac{-U_b}{RT} + \frac{-zF\delta E}{RT}\right) = b_b \exp\left(\frac{-zF\delta E}{RT}\right), \quad \text{(A1)}$$

where a_b is the partition coefficient for a given ion into the membrane, and $b_b = (-U_b/RT)$. The equilibrium constant, K_m, for the ion translocation reaction is equal to

$$K_m = \frac{[\text{ion}]_{\text{site}}}{[\text{ion}]_1[\text{ion}]_2} = \frac{\text{dissociation energy}}{\text{association energy}}, \quad \text{(A2)}$$

regardless of the number of sites within the membrane, because the total energy required for one ion to translocate across the membrane will always be $\Sigma - U_b$ [$= \int(\mathrm{d}(-U_b)/\mathrm{d}x)$] for all internal membrane barriers. The probability that a site is not occupied, P_{NO}, will, similarly, always equal

$$P_{NO} = \frac{\sum \text{dissociation energy}}{\sum \text{association energy} + \sum \text{dissociation energy}}. \quad \text{(A3)}$$

It follows that the fraction of sites not occupied in the presence of an ion relative to its absence will always equal

$$\frac{P_{NO}([TAA])}{P_{NO}(0)} = \frac{K_m}{[TAA] + K_m} = \frac{1}{[TAA]/K_m + 1}, \quad \text{(A4)}$$

because the dissociation energies are concentration-independent and the association energies are concentration dependent. The expression for K_m will vary depending on the number of sites (and barriers) encountered by the ion when translocating through the channel and were derived for the three energy profiles illustrated in Fig. 6. This expression does not require that the blocking site for TAA^+ ions be identical to the monovalent cation selectivity filter for the permeant earth alkali metal ions plus TMA^+ and TEA^+, as reported previously for the homotypic rCx40 channel (Beblo and Veenstra, 1997). Eq. A4 also only applies to the unilateral addition of TAA^+, because $P_{NO}(0)$ was obtained by reversing V_j polarity (negative V_j in the TAA^+-containing cell 1) resulting in net cationic efflux from the high $[K^+]$, zero $[TAA^+]$ cell (cell 2) for the experiments described in Figs. 1–10.

One-site, two-barrier model

This is analogous to the original Woodhull (1973) derivation with two exceptions: 1) that the transjunctional potential is defined with the opposite convention to that used for an external blocking ion entering the channel pore and 2) that the channel is now symmetrical to model a homotypic gap-junction channel (Fig. 6 *A*). Therefore, the signs are reversed in the exponential terms of the expressions and $b_1 = b_2$, etc. in relation to the original Woodhull (1973) derivation. The energy barriers are

$$k_1 = b_1\left[[TAA]_1 \exp\left(\frac{zF\delta V_j}{2RT}\right) + [TAA]_2 \exp\left(\frac{-zF(1-\delta)V_j}{2RT}\right)\right]$$

and

$$k_{-1} = b_{-1}\left[\exp\left(\frac{-zF\delta V_j}{2RT}\right) + \exp\left(\frac{zF(1-\delta)V_j}{2RT}\right)\right].$$

By definition, $K_m = k_{-1}/k_1$, and, solving for K_m,

$$K_m = \left(\frac{b_{-1}}{b_1}\right)\exp\left(\frac{-zF\delta V_j}{RT}\right) + \left(\frac{b_{-1}}{b_1}\right)\exp\left(\frac{zF(1-2\delta)V_j}{2RT}\right) + [TAA]_2 \exp\left(\frac{-zF(1-2\delta)V_j}{2RT}\right), \quad \text{(A5)}$$

because $K_m = [TAA^+]_1$ at equilibrium and $-K_m = [TAA^+]_2$ (negative because it refers to the opposite side of the channel). For the unilateral

addition of the blocking TAA^+ ions to cell 1 as described in the experimental protocols, the K_m for a single binding site becomes

$$K_m = \left(\frac{b_{-1}}{b_1}\right)\exp\left(\frac{-zF\delta V_j}{RT}\right) + \left(\frac{b_{-1}}{b_1}\right)\exp\left(\frac{zF(1-2\delta)V_j}{2RT}\right), \quad \text{(A6)}$$

if TAA^+ is permeant. If it is assumed that the TAA^+ ions are not permeant, this expression reduces to

$$K_m = \left(\frac{b_{-1}}{b_1}\right)\exp\left(\frac{-zF\delta V_j}{RT}\right), \quad \text{(A7)}$$

which is identical to the original Woodhull (1973) derivation, except for the sign change due to the convention commonly used to define V_j. For a heterotypic gap-junction channel, $k_1 \neq k_2$ and $k_{-1} \neq k_{-2}$, and the solutions to the Fig. 6 *A* diagram are

$$K_m = \left(\frac{b_{-1}}{b_1}\right)\exp\left(\frac{-zF\delta V_j}{RT}\right) + \left(\frac{b_{-2}}{b_1}\right)\exp\left(\frac{zF(1-2\delta)V_j}{2RT}\right) + [TAA]_2\left(\frac{b_2}{b_1}\right)\exp\left(\frac{-zF(1-2\delta)V_j}{2RT}\right) \quad \text{(A8)}$$

and

$$K_m = \left(\frac{b_{-1}}{b_1}\right)\exp\left(\frac{-zF\delta V_j}{RT}\right) + \left(\frac{b_{-2}}{b_1}\right)\exp\left(\frac{zF(1-2\delta)V_j}{2RT}\right). \quad \text{(A9)}$$

Under bilateral $[TAA^+]$ conditions, the K_m must be determined by Eq. A5. Additionally, the solution for P_{NO} according to Eq. A3 has the general solution,

$$P_{NO} = \frac{K_m[TAA]_2 = 0/K_m[TAA]_2 \neq 0}{1 + [TAA]_1/K_m[TAA]_2 \neq 0}, \quad \text{(A10)}$$

which has the exact solution

$$P_{NO} = \frac{\text{(Eq. A6 or A9)/(Eq. A5 or A8)}}{1 + [TAA]_1/\text{(Eq. A5 or A8)}} \quad \text{(A11)}$$

for the one-site model.

Two-site model

The model energy diagrams for a symmetrical two-site channel depend on whether it is assumed that the two sites are independent or whether they interact to form a composite (common) energy profile in the channel interior between the two sites. The different energy profiles are illustrated in Fig. 6, *B* (composite) and *C* (independent).

Three-barrier

There must be a physical separation of some kind between the two internal binding sites, which are represented by the energy barrier with values of k_2 and k_{-2} in Fig. 6 *B*. In this case, k_1 and k_{-1} will have the same values as before provided that the two sites are identical. This assumption is inherent for a homotypic gap-junction channel. The internal association energy for site 1 (δ) is

$$k_{-2} = b_{-2}\exp\left(\frac{-zF(1-2\delta)V_j}{2RT}\right),$$

and the internal association energy for site 2 ($1 - \delta$) is

$$k_2 = b_2\exp\left(\frac{zF(1-2\delta)V_j}{2RT}\right).$$

The value of k_2 and k_{-2} determine whether the ions in the pore have the same, less, or more energy than in bulk aqueous solution. For a symmetrical channel, $k_2 = k_{-2}$, and the equilibrium constant for the ion distribution between the two internal sites becomes

$$k_2 = b_2\left[\frac{\exp(zF(1-2\delta)V_j/RT) + 1}{\exp(zF(1-2\delta)V_j/2RT)}\right].$$

From Eq. A2, it follows that $K_m = k_{-1}/(k_1 + k_2)$ or

$$K_m = \left(\frac{b_{-1}}{b_1}\right)\left[\exp\left(\frac{-zF\delta V_j}{RT}\right) + \exp\left(\frac{zF(1-2\delta)V_j}{2RT}\right)\right] + [TAA]_2\exp\left(\frac{-zF(1-2\delta)V_j}{2RT}\right) + \left(\frac{b_2}{b_1}\right)[TAA]_2\left[\frac{\exp(zF(1-3\delta)V_j/RT) + 1}{\exp(zF(1-3\delta)V_j/2RT)}\right]. \quad \text{(A12)}$$

If $[TAA^+]_2 = 0$, then this expression again reduces to Eq. A6 if TAA^+ is permeable and to Eq. A7 if TAA^+ is impermeant. Assuming $k_1 \neq k_3$ and $k_{-1} \neq k_{-3}$ represents the heterotypic case to Fig. 6 *B*, the complete solution to this barrier model is

$$K_m = \left(\frac{b_{-1}}{b_1}\right)\exp\left(\frac{-zF\delta V_j}{RT}\right) + \left(\frac{b_{-3}}{b_1}\right)\exp\left(\frac{zF(1-2\delta)V_j}{2RT}\right) + [TAA]_2\left(\frac{b_3}{b_1}\right)\exp\left(\frac{-zF(1-2\delta)V_j}{2RT}\right) + \left(\frac{b_2}{b_1}\right) \cdot [TAA]_2\left[\frac{\exp(zF(1-3\delta)V_j/RT) + 1}{\exp(zF(1-3\delta)V_j/2RT)}\right], \quad \text{(A13)}$$

which reduces to Eq. A6 (by substituting b_{-3} for b_{-2}).

The bilateral addition of TAA^+ requires that

$$P_{NO} = \frac{\text{(Eq. A6 or A9)/(Eq. A12 or A13)}}{1 + [TAA]_1/\text{(Eq. A12 or A13)}} \quad \text{(A14)}$$

for the two-site, three-barrier model. The reason the $K_m(V_j)$ for unilateral addition of TAA^+ is the same as for the one-site model and the two-site, three-barrier model is that any internal TAA^+ ions must be associated with a site.

Four barrier

This two-site, four-barrier model assumes that there is a central compartment where any permeant ions would assume the same relative energy as

in bulk solution. The energy profile is illustrated in Fig. 6 *C*. The internal association energy becomes

$$k_{-2} = b_{-2}[\mathrm{TAA}]_{\mathrm{pore}}\left[\frac{\exp(zF(1-2\delta)V_j/RT)+1}{\exp(zF(1-2\delta)V_j/2RT)}\right],$$

the dissociation energy becomes

$$k_2 = b_2\left[\frac{\exp(zF(1-2\delta)V_j/RT)+1}{\exp(zF(1-2\delta)V_j/2RT)}\right],$$

and the equilibrium constant becomes

$$K_m = \frac{k_{-1}+k_2}{k_1+k_{-2}}.$$

This expression is analogous to the three-barrier model except for the inclusion of a $[\mathrm{TAA}^+]_{\mathrm{pore}}$ term and $k_2 \neq k_{-2}$. Hence, the derivations will be identical except for the two relative differences in the k_{-2} and k_2 terms. Solving for K_m, we obtain

$$K_m = \left(\frac{b_{-1}}{b_1}\right)\left[\exp\left(\frac{-zF\delta V_j}{RT}\right)+\exp\left(\frac{zF(1-2\delta)V_j}{2RT}\right)\right] + [\mathrm{TAA}]_2\exp\left(\frac{-zF(1-2\delta)V_j}{2RT}\right)+\left[\left(\frac{b_2}{b_1}\right)+\left(\frac{b_{-2}}{b_1}\right)\cdot[\mathrm{TAA}]_2\right]\left[\frac{\exp(zF(1-3\delta)V_j/RT)+1}{\exp(zF(1-3\delta)V_j/2RT)}\right] \quad (A15)$$

for the four-barrier model where $[\mathrm{TAA}^+]_{\mathrm{pore}} = [\mathrm{TAA}^+]_2$. If $[\mathrm{TAA}^+]_2 = 0$, then the expression reduces to

$$K_m = \left(\frac{b_{-1}}{b_1}\right)\left[\exp\left(\frac{-zF\delta V_j}{RT}\right)+\exp\left(\frac{zF(1-2\delta)V_j}{2RT}\right)\right] + \left(\frac{b_2}{b_1}\right)\left[\frac{\exp(zF(1-3\delta)V_j/RT)+1}{\exp(zF(1-3\delta)V_j/2RT)}\right]. \quad (A16)$$

If $[\mathrm{TAA}^+]$ is impermeant, then this expression again reduces to Eq. A7. Assuming $k_1 \neq k_3$, $k_{-1} \neq k_{-3}$, $k_2 \neq k_4$, and $k_{-2} \neq k_{-4}$, represents the heterotypic case to Fig. 6 *C*, the complete solution to this barrier model is

$$K_m = \left(\frac{b_{-1}}{b_1}\right)\exp\left(\frac{-zF\delta V_j}{RT}\right)+\left(\frac{b_{-3}}{b_1}\right)\exp\left(\frac{zF(1-2\delta)V_j}{2RT}\right) + [\mathrm{TAA}]_2\left(\frac{b_3}{b_1}\right)\exp\left(\frac{-zF(1-2\delta)V_j}{2RT}\right) + \left[\left(\frac{b_2}{b_1}\right)+\left(\frac{b_{-4}}{b_1}\right)[\mathrm{TAA}]_2\right]\exp\left(\frac{zF(1-3\delta)V_j}{2RT}\right) + \left[\left(\frac{b_4}{b_1}\right)+\left(\frac{b_{-2}}{b_1}\right)[\mathrm{TAA}]_2\right]\exp\left(\frac{-zF(1-3\delta)V_j}{2RT}\right), \quad (A17)$$

which reduces to

$$K_m = \left(\frac{b_{-1}}{b_1}\right)\exp\left(\frac{-zF\delta V_j}{RT}\right)+\left(\frac{b_{-3}}{b_1}\right)\exp\left(\frac{zF(1-2\delta)V_j}{2RT}\right) + \left(\frac{b_2}{b_1}\right)\exp\left(\frac{zF(1-3\delta)V_j}{2RT}\right) + \left(\frac{b_4}{b_1}\right)\exp\left(\frac{-zF(1-3\delta)V_j}{2RT}\right), \quad (A18)$$

when $[\mathrm{TAA}]_2 = 0$. The bilateral addition of TAA^+ requires that

$$P_{\mathrm{NO}} = \frac{(\text{Eq. A16 or A18})/(\text{Eq. A15 or A17})}{1+[\mathrm{TAA}]_1/(\text{Eq. A15 or A17})} \quad (A19)$$

These expressions state that the internal equilibrium between sites 1 and 2 depends on $[\mathrm{TAA}^+]_1$, $[\mathrm{TAA}^+]_2$, and $(1-3\delta)V_j$. Because b_{-2} and b_2 can only be estimated from the theoretical fit of the $K_m(V_j)$ data, there is no definitive way to tell the difference between the two internal energy diagrams from unilateral TAA^+ experiments. If TAA^+ is impermeant, Eq. A12 and A15 reduce to Eq. A5/A8 under bilateral TAA^+ conditions. Thus, it is not possible to distinguish between the one-site and two-site barrier models if blockade by TAA^+ is independent of *trans* $[\mathrm{TAA}^+]$. If TAA^+ is permeant, the differences between the two-site, three- and four-barrier models still depend entirely on the k_{-2} and k_2 terms under bilateral TAA^+ conditions. In conclusion, determination of the internal energy profile of a symmetrical gap-junction channel requires an impermeant blocker and the presence of *cis–trans* interactions by the blocking ions to delineate between one or two sites. If different K_m are evident for two distinct homotypic gap-junction channels, the heterotypic approach will produce a more definitive test of the one- or two-site models using the derivations, provided that the K_m is measured for each side from unilateral blocking ion experiments.

We want to thank Sophia Tashkovski, Stephanie DiPerna, Lynette Santana, Nan Pan, Michelle Kuhfta, and Erica Deibert for their technical assistance in the preparation and maintenance of the Cx40-transfected N2A cells. Dr. Eric C. Beyer graciously provided the rat Cx40 cDNA. We thank Drs. Jeffrey Freedman and Jack Sullivan for their comments during the completion of this research and Dr. Sullivan for his reading of the manuscript.

This work was supported by National Institutes of Health, Heart, Lung and Blood Institute grants HL-42220 to R.D.V. and HL-45466 to R.D.V. and E.C.B.

REFERENCES

Anderson, C. S., R. MacKinnon, C. Smith, and C. Miller. 1988. Charybdotoxin block of single Ca^{2+}-activated K^+ channels. Effects of channel gating, voltage, and ionic strength. *J. Gen. Physiol.* 91:317–333.

Anumonwo, J. M. B., S. M. Taffet, H. Gu, M. Chanson, A. P. Moreno, and M. Delmar. 2001. The carboxyl terminal domain regulates the unitary conductance and voltage dependence of connexin40 gap junction channels. *Circ. Res.* 88:666–673.

Armstrong, C. M. 1971. Interaction of tetraethylammonium ion derivatives with the potassium channels of giant axons. *J. Gen. Physiol.* 58: 413–437.

Armstrong, C. M., and L. Binstock. 1965. Anomalous rectification in squid giant axon with tetraethylammonium chloride. *J. Gen. Physiol.* 48: 859–872.

Baldwin, K. M. 1979. Cardiac gap junction configuration after an uncoupling treatment as a function of time. *J. Cell Biol.* 82:66–75.

Bastiannse, L. E. M., H. J. Jongsma, A. van der Laarse, and B. R. Takens-Kwak. 1993. Heptanol-induced decrease in cardiac gap junction conductance is mediated by a decrease in the fluidity of membraneous cholesterol-rich domains. *J. Membr. Biol.* 136:135–145.

Beblo, D. A., and R. D. Veenstra. 1997. Monovalent cation permeation through the connexin40 gap junction channel. Cs, Rb, K, Na, Li, TEA, TMA, TBA, and effects of anions Br, Cl, F, acetate, aspartate, glutamate, and NO_3. *J. Gen. Physiol.* 109:509–522.

Beblo, D. A., H.-Z. Wang, E. C. Beyer, E. M. Westphale, and R. D. Veenstra. 1995. Unique conductance, gating, and selective permeability properties of gap junction channels formed by connexin40. *Circ. Res.* 77:813–822.

Blaustein, R. O., and A. Finkelstein. 1990a. Voltage-dependent block of anthrax toxin channels in planar phospholipid bilayer membranes by symmetric tetraalkylammonium ions. Effects on macroscopic conductance. *J. Gen. Physiol.* 96:905–919.

Blaustein, R. O., and A. Finkelstein. 1990b. Diffusion limitation in the block by symmetric tetraalkylammonium ions of anthrax toxin channels in planar phospholipid bilayer membranes. *J. Gen. Physiol.* 96:943–957.

Blaustein, R. O., E. J. A. Lea, and A. Finkelstein. 1990. Voltage-dependent block of anthrax toxin channels in planar phospholipid bilayer membranes by symmetric tetraalkylammonium ions. Single-channel analysis. *J. Gen. Physiol.* 96:921–942.

Burt, J. M. 1989. Uncoupling of cardiac cells by doxyl stearic acids: specificity and mechanism of action. *Am. J. Physiol. Cell Physiol.* 256:C913–C924.

Burt, J. M., and D. C. Spray. 1989. Volatile anesthetics block intercellular communication between neonatal rat myocardial cells. *Circ. Res.* 65: 829–837.

Choi, K. L., C. Mossman, J. Aubé, and G. Yellen. 1993. The internal quaternary ammonium receptor site of *Shaker* potassium channels. *Neuron.* 10:533–541.

Davidson, J. S., and I. M. Baumgarten. 1988. Glycyrrhetinic acid derivatives: a novel class of inhibitors of gap-junctional intercellular communication. Structure–activity relationships. *J. Pharmacol. Exp. Ther.* 246:1104–1107.

French, R. J., and J. J. Shoukimas. 1985. An ion's view of the potassium channel. The structure of the permeation pathway as sensed by a variety of blocking ions. *J. Gen. Physiol.* 85:669–698.

Guan, X., B. F. Cravatt, G. R. Ehring, J. E. Hall, D. L. Boger, R. A. Lerner, and N. B. Gilula. 1997. The sleep-inducing lipid oleamide deconvolutes gap junction communication and calcium wave transmission in glial cells. *J. Cell Biol.* 139:1785–1792.

Halpern, M., Y. Sasson, and M. Rabonovitz. 1982. Hydroxide ion initiated reactions under phase transfer catalysis conditions—IV. Effect of catalyst structure. *Tetrahedron.* 38:3183–3187.

Hille, B. 1992. Ionic Channels of Excitable Membranes. 2nd edition. Sinauer Associates, Inc., Sunderland, MA. 429–436.

Holmgren, M., M. E. Jurman, and G. Yellen. 1996. N-type inactivation and the S4–S5 region of the *Shaker* K^+ channel. *J. Gen. Physiol.* 108: 195–206.

Hurst, R. S., R. Latorre, L. Toro, and E. Stefani. 1995. External barium block of *Shaker* potassium channels: evidence for two binding sites. *J. Gen. Physiol.* 106:1069–1087.

Johnston, M. F., S. A. Simon, and F. Ramon. 1980. Interaction of anaesthetics with electrical synapses. *Nature.* 286:498–500.

Lundbæk, J. A., and O. S. Andersen. 1999. Spring constants for channel-induced lipid bilayer deformations. Estimates using gramicidin channels. *Biophys. J.* 76:889–895.

MacKinnon, R., and C. Miller. 1988. Mechanism of charybdotoxin block of the high-conductance, Ca^{2+}-activated K^+ channel. *J. Gen. Physiol.* 91:335–349.

MacKinnon, R., and G. Yellen. 1990. Mutations affecting TEA blockade and ion permeation in voltage-activated K^+ channels. *Science.* 250: 276–279.

Manivannan, K., S. V. Ramanan, R. T. Mathias, and P. R. Brink. 1992. Multichannel recordings from membranes which contain gap junctions. *Biophys. J.* 61:216–227.

Newland, C. F., J. P. Adelman, B. L. Tempel, and W. Almers. 1992. Repulsion between tetraethylammonium ions in cloned voltage-gated potassium channels. *Neuron.* 8:975–982.

Peracchia, C. 1977. Gap Junctions. Structural changes after uncoupling procedures. *J. Cell Biol.* 72:628–641.

Perkins, G., D. Goodenough, and G. Sosinsky. 1997. Three-dimensional structure of the gap junction connexon. *Biophys. J.* 72:533–544.

Robinson, R. A., and R. H. Stokes. 1965. Electrolyte Solutions. 2nd edition. Butterworth, London, U.K. 125.

Sanchez, D. Y., and A. L. Blatz. 1995. Block of neuronal chloride channels by tetraethylammonium ion derivatives. *J. Gen. Physiol.* 106: 1031–1046.

Sanchez, J. A., J. A. Dani, D. Siemen, and B. Hille. 1986. Slow permeation of organic cations in acetylcholine receptor channels. *J. Gen. Physiol.* 87:985–1001.

Spray, D. C., and J. M. Burt. 1990. Structure-activity relations of the cardiac gap junction channel. *Am. J. Physiol. Cell Physiol.* 258: C195–C205.

Takens-Kwak, B. R., H. J. Jongsma, M. B. Rook, and A. C. G. van Ginneken. 1992. Mechanism of heptanol-induced uncoupling of cardiac gap junctions: a perforated patch-clamp study. *Am. J. Physiol. Cell Physiol.* 262:C1531–C1538.

Tinker, A., A. R. G. Lindsay, and A. J. Williams. 1992. Large tetraalkyl ammonium cations produce a reduced conductance state in the sheep cardiac sarcoplasmic reticulum Ca^{2+}-release channel. *Biophys. J.* 61: 1122–1132.

Trexler, E. B., M. V. L. Bennett, T. A. Bargiello, and V. K. Verselis. 1996. Voltage gating and permeation in a gap junction hemichannel. *Proc. Natl. Acad. Sci. U.S.A.* 93:5836–5841.

Unger, V. M., N. M. Kumar, N. B. Gilula, and M. Yeager. 1999. Three-dimensional structure of a recombinant gap junction membrane channel. *Science.* 283:1176–1180.

Veenstra, R. D. 2000. Ion permeation through connexin gap junction channels: effects on conductance and selectivity. *In* Current Topics in Membranes, Vol. 49, Gap Junctions: Molecular Basis of Cell Communication in Health and Disease. C. Peracchia, editor. Academic Press, San Diego, CA. 95–129.

Veenstra, R. D. 2001. Voltage clamp limitations of dual whole-cell gap junction current and voltage recordings. I. Conductance measurements. *Biophys. J.* 80:2231–2247.

Veenstra, R. D., and R. L. DeHaan. 1988. Regulation of single channel activity in cardiac gap junctions. *In* Cell Interactions and Gap Junctions, Volume II. N. Sperelakis and W. C. Cole, editors. CRC Press, Boca Raton, FL. 65–83.

Veenstra, R. D., and P. R. Brink. 1992. Patch clamp analysis of gap junctional currents. *In* Cell–Cell Interactions: A Practical Approach. B. Stevenson, D. L. Paul, and W. Gallin, editors. IRL Press, Oxford, U.K. 167–201.

Veenstra, R. D., and H.-Z. Wang. 1998. Biophysics of gap junction channels. *In* Heart Cell Communication in Health and Disease. W. C. DeMello and M. Janse, editors. Kluwer Academic, Norwell, MA. 73–103.

Wang, H.-Z., and R. D. Veenstra. 1997. Monovalent ion selectivity sequences of the rat connexin43 gap junction channel. *J. Gen. Physiol.* 109:491–507.

Woodhull, A. M. 1973. Ionic blockage of sodium channels in nerve. *J. Gen. Physiol.* 61:687–708.

Wu, J., J. McHowat, J. E. Saffitz, K. A. Yamada, and P. B. Corr. 1993. Inhibition of gap junctional conductance by long-chain acylcarnitines and their preferential accumulation in junctional sarcolemma during hypoxia. *Circ. Res.* 72:879–889.

Yellen, G. 1987. Permeation in potassium channels: implications for channel structure. *Ann. Rev. Biophys. Biophys. Chem.* 16:227–246.

Zhang, Y., D. W. McBride, Jr., and O. P. Hamill. 1998. The ion selectivity of a membrane conductance inactivated by extracellular calcium in *Xenopus* oocytes. *J. Physiol. (Lond.).* 508:763–776.